

**MODELING OF GROWTH KINETICS OF WET GRANULATION IN A HIGH
SHEAR MIXER BY MEANS OF IMAGE PROCESSING AND ANALYSIS**

By

Alvaro Realpe Jiménez

A thesis submitted in partial fulfillment of the requirements for the degree of

DOCTOR OF PHILOSOPHY
in
CHEMICAL ENGINEERING

UNIVERSITY OF PUERTO RICO
MAYAGÜEZ CAMPUS

2006

Approved by:

Carlos Velázquez Figueroa, Ph.D
President, Graduate Committee

Date

Rodolfo Romañach Suárez, Ph.D
Member, Graduate Committee

Date

Nelson Cardona Martínez, Ph.D
Member, Graduate Committee

Date

David Suleiman Rosado, Ph.D
Member, Graduate Committee

Date

Gustavo E. López, PhD
Representative of Graduate Studies

Date

Nelson Cardona Martínez, Ph.D
Chairperson of the Department

Date

ABSTRACT

Wet granulation is one of the most important operations where fine particles are agglomerated into larger granules by adding a binder. The process is used in many chemical industries including pharmaceutical, mineral processing, agricultural, and detergents. In spite of its importance and many years of research, the understanding of the granulation process is still quite limited. The main objective of this research is to study the effects of initial particle size distribution (PSD) shape (unimodal versus bimodal), initial particle size, and the amount and viscosity of binder on growth kinetics and the mechanism of wet granulation, and to model the agglomeration mechanism of particles, using the population balance equation (PBE) and considering the initial properties of binder and particles.

This research was carried out in three different phases. Initially, an image processing and analysis algorithm was validated and used to determine the PSD during the wet granulation. The test of the vision system capability to determine particle size indicated high precision with a repeatability of 0.0012 in and 0.5% relative standard deviation. Near-infrared (NIR) spectroscopy method was validated and used, at the same time, to determine the moisture content.

In the second phase, several variables were investigated. The Split-Plot experimental design with three factors (amount, viscosity of binder, and initial PSD) and three levels for each factor was carried out. The variation of these three factors are consistent with the viscous Stokes' (St_v) number developed by Ennis et al. [1991]. The effect of initial PSD shape, unimodal versus bimodal, on the growth kinetics and mechanism of wet granulation were also evaluated.

Wet granulation of pharmaceutical powders with initial bimodal PSD presented growth kinetics in two stages. The first stage of granule growth is fast, similar to a non-inertial regime found by Adetayo et al. [1995]. This stage is controlled by binder amount and the high probability of coalescence because of collisions of small and large particles that increase the growth rate, as indicated by coalescence kernels published in the literature. The second

stage is characterized by slow agglomeration of particles with a water content 13.6% v/w, and slow breakage of particles with water contents of 9.9 and 11.7% v/w. In contrast, wet granulation of pharmaceutical powders with initial unimodal PSD exhibited slow growth kinetics consisting of one stage because high concentration of particles of similar size decreases the probability of granule coalescence, as compared to the high coalescence probability between collisions of small and large particles.

In the last phase, an agglomeration model between small and large particles was developed based on diffusion of small particles to a larger one through binder layer on the particle surface. Furthermore, coalescence kernels with physical interpretation have been developed for each stage of wet granulation. The coalescence kernel of slow growth rate accurately describes the PSD during wet granulation process.

RESUMEN

La granulación húmeda es una de las operaciones unitarias más importantes donde por adición de un líquido las partículas finas son aglomeradas para formar una partícula de mayor tamaño. Este proceso es usado en muchas industrias químicas incluyendo la farmacéutica, procesamiento de minerales, agricultura, y detergentes. A pesar de su importancia y muchos años de investigación, el entendimiento del proceso de granulación es todavía limitado. El principal objetivo de esta investigación es estudiar el efecto de: la forma inicial de la distribución de tamaño de partículas (unimodal versus bimodal), el tamaño de partículas, y la cantidad y viscosidad de líquido sobre la cinética de crecimiento y el mecanismo de la granulación húmeda; y a su vez modelar el mecanismo de aglomeración de partículas, usando la ecuación de balance de población (PBE) y considerando las propiedades iniciales del líquido y de las partículas.

Esta investigación fue realizada en tres etapas. Inicialmente, un algoritmo para procesar y analizar imágenes fue validado y usado para determinar la distribución de tamaño de partículas durante la granulación húmeda. La prueba de capacidad del sistema de visión para determinar el tamaño de las partículas indicó alta precisión con una capacidad de repetición de 0.0012 pulgadas y una desviación estándar relativa de 0.5%. A la misma vez, un método de espectroscopía de infrarojo cercano fue validado y usado para determinar el contenido de humedad.

En la segunda etapa, varias variables fueron investigadas. El diseño experimental “Split-plot” con tres factores (cantidad y viscosidad de líquido, y distribución inicial de tamaño de partículas) y tres niveles para cada factor fue realizado. La variación de estos tres factores son consistentes con el número de Stokes viscoso desarrollado por Ennis et al. [1991]. El efecto de la forma inicial de la distribución de tamaño de partículas, unimodal versus bimodal, también fue evaluado sobre la cinética de crecimiento y el mecanismo de la granulación húmeda.

La granulación húmeda de polvos farmacéuticos con distribución de tamaño de partículas de forma inicial bimodal presentó cinética de crecimiento en dos etapas. La

primera etapa de crecimiento de los gránulos es rápida, similar al régimen no-inercial encontrado por Adetayo et al. [1995]. Esta etapa es controlada por la cantidad de líquido y la alta probabilidad de unión debido a la colisión de partículas pequeñas y grandes que incrementa la tasa de crecimiento, como indican las ecuaciones fundamentales de unión de gránulos publicados en la literatura. La segunda etapa es caracterizada por una lenta aglomeración de partículas con 13.6% v/w de contenido de agua, y lento rompimiento de partículas con contenido de agua de 9.9 y 11.7% v/w. Opuestamente, la granulación húmeda de polvos farmacéuticos con distribución de tamaño de partículas de forma inicial unimodal exhibe a lenta cinética de crecimiento de una etapa, porque la alta concentración de partículas de tamaño similar disminuye la probabilidad de unión de los gránulos, en comparación a la alta probabilidad de unión entre colisiones de partículas pequeñas y grandes.

Finalmente, un modelo de aglomeración entre partículas pequeñas y grandes fue desarrollado basado en la difusión de partículas pequeñas hacia una partícula grande a través de la capa de líquido alrededor de la superficie de las partículas. Además, para cada etapa de la granulación húmeda se desarrollaron ecuaciones fundamentales de aglomeración de gránulos con interpretación física. La ecuación fundamental de aglomeración para tasa de crecimiento lenta describe con exactitud la distribución del tamaño de partículas durante el proceso de granulación.

DEDICATION

To my son Marco Antonio Realpe.

To my darling daughter Valentina Realpe.

To my parents Luz Marina and Alberto.

ACKNOWLEDGEMENTS

First of all, I wish to express my sincere gratitude to my advisor, Dr. Carlos Velázquez Figueroa, for giving me the opportunity to work with him, for trusting my capabilities and for his unreserved support through the entire project. Without his knowledge, enthusiasm and encouragement to publish papers, this project would not have been possible.

Special thanks to Dr. Rodolfo Romañach and Dr. Nelson Cardona for their support, their investment of time, their teaching, their encouragement to publish papers and their motivation to participate in classes with discussions, answers and questions. Participations during classes were very important for my personal and professional formation.

I am grateful to all students (undergraduate and graduate) for all the collaboration during the validation process of the vision system, to Angel Zapata and Efren Gregory for their collaboration during the equipment setup, and to Dr. Wulkow and co-workers for their support with software and useful comments on agglomeration process.

The Chemical Engineering Department, the National Science Foundation and the Experimental Program to Stimulate Competitive Research (NSF-EPSCoR), and CPPR are acknowledged for financial support. The Chemical Engineering Department is thanked for giving the opportunity to use their facilities. I would like to thank the staff at the Chemical Engineering Department for welcoming me to the Department.

Table of Contents

ABSTRACT.....	II
RESUMEN	IV
ACKNOWLEDGEMENTS.....	VII
TABLE OF CONTENTS	VIII
LIST OF TABLES.....	X
LIST OF FIGURES	XI
1 INTRODUCTION.....	2
1.1 JUSTIFICATION.....	2
1.2 OBJECTIVES.....	3
2 PATTERN RECOGNITION FOR CHARACTERIZATION OF PHARMACEUTICAL POWDERS	4
2.1 INTRODUCTION.....	4
2.2 EXPERIMENTAL: SAMPLES, EQUIPMENTS AND PROCEDURE.....	5
2.2.1 Particle Size Determination of Wet Granules.....	7
2.2.2 Experimental Design	7
2.3 IMAGE PROCESSING AND ANALYSIS	9
2.4 RESULTS AND DISCUSSION	12
2.4.1 Statistical validation in determining particle size using spherical shape.....	12
2.4.2 Statistical validation of pattern recognition technique for determination of shape and its size...	13
2.4.3 Morphological characterization of pharmaceutical powders.....	15
2.5 CONCLUSIONS.....	17
3 EFFECT OF PARTICLE AND BINDER CHARACTERISTICS ON THE GROWTH KINETICS AND MECHANISM OF WET GRANULATION.....	18
3.1 INTRODUCTION.....	18
3.2 EXPERIMENTAL METHODS.....	21
3.2.1 Materials and equipments.....	21
3.2.2 Granulator Characterization.....	24
3.2.3 Granulation Process.....	25
3.2.4 Experimental Design	26
3.3 DEVELOPMENT OF THE CALIBRATION MODEL FOR MOISTURE CONTENT DETERMINATION	26
3.4 RESULTS AND DISCUSSION	27
3.4.1 Effect of initial PSD shape (unimodal versus bimodal) on the mechanism and growth rate of wet granulation.....	27
3.4.2 Effect of Initial Particle Size on Granule Growth Rate in Wet Granulation	30

3.4.3	<i>Effect of binder content on granule growth and the mechanism of wet granulation</i>	31
3.4.4	<i>Effect of Binder Viscosity on Granule Growth and the Mechanism of Wet Granulation</i>	36
3.4.4.1	<i>Effect of High Binder Viscosity and High Binder Content on the Wet Granulation Process</i>	41
3.4.5	<i>Description of Experimental Data, using the Agglomeration Kernels Proposed in the Literature</i> ..	44
3.5	CONCLUSIONS.....	46
4	AGGLOMERATION MODELING OF SMALL AND LARGE PARTICLES BY A DIFFUSION THEORY APPROACH	48
4.1	INTRODUCTION.....	48
4.2	DEVELOPMENT OF AGGLOMERATION KERNEL: THEORETICAL ANALYSIS	50
4.2.1	<i>Agglomeration of Particles</i>	50
4.2.2	<i>Agglomeration Mechanism based on Brownian Movement and Viscous Forces</i>	53
4.2.2.1	<i>Modeling the First Stage of Fast Granule Growth of Wet Granulation</i>	54
4.2.2.2	<i>Modeling the Stage of Slow Granule Growth of Wet Granulation</i>	55
4.3	SOLUTION OF THE POPULATION BALANCE EQUATION.....	56
4.4	RESULTS AND DISCUSSION	57
4.4.1	<i>Comparison of model simulation to experimental data</i>	58
4.4.1.1	<i>First Stage of Wet Granulation</i>	58
4.4.1.2	<i>Second Stage of Wet Granulation</i>	58
4.5	CONCLUSIONS.....	66
	REFERENCES.....	67
5	RECOMMENDATIONS AND FUTURE WORK	72
5.1	RECOMMENDATIONS	72
5.2	FUTURE WORK.....	73
APPENDIX A.	CALIBRATION MODEL FOR MOISTURE CONTENT DETERMINATION	74
APPENDIX B.	MASS MEDIAN DIAMETER (MMD)	77

List of Tables

Tables	Page
Table 2.1 Equipments and software used to acquire and analyze images	6
Table 2.2 Study of repeatability of metal bead	12
Table 2.3 Study of repeatability for images with particles without contact	13
Table 2.4 Study of repeatability for images with particles in contact	14
Table 3.1 Study of repeatability	25
Table 3.2 Experimental Design	26
Table 3.3 Effect of particle size on granule growth rate at 13.6% v/w and 1cp viscosity	30
Table 3.4 Effect of binder viscosity on granule growth rate at 11.7% v/w and coarse size powders (PSD3)	37
Table 3.5 Goodness of fit for kernels, relative to the experimental data	45
Table 4.1 Size-dependent kernels obtained empirically, semi-empirically or from semi- theoretical concepts	50
Table 4.2 Experimental Design	58
Table 4.3 Fitting the coalescence kernels to the experimental data	60
Table B.0.1 Mass median diameter for each combination of factors and levels	77
Table B.0.2 Analysis of variance (ANOVA) for mass median diameter measurements	78

List of Figures

Figures	Page
Figure 2.1 Vision System Schematic	6
Figure 2.2 The 3 ² design for determination of the vision system capability	8
Figure 2.3 Synthetic images of different forms and sizes with particles (a) without contact and (b) in contact.	8
Figure 2.4 Real shape of (a) Microcrystalline cellulose and (b) lactose monohydrate.....	9
Figure 2.5 Schematic flow of algorithm for image processing and analysis.....	10
Figure 2.6 Synthetic images separated and classified (a) circular particles (c) acicular particle with R=10 (d) acicular particles with R=5 (R=length /breadth).....	14
Figure 2.7 Image Processing steps for (a) microcrystalline cellulose and (e) saccharose.....	15
Figure 2.8 Change of standard deviation of each template versus number of particles	16
Figure 3.1 Layering growth mechanism proposed by Tardos et al. (1997).....	21
Figure 3.2 Initial particle size distributions for wet granulation.....	22
Figure 3.3 Laboratory-scale high shear mixer	23
Figure 3.4 Zones inside the granulator	24
Figure 3.5 Cumulative mass percentages for the four different zones inside the granulator..	25
Figure 3.6 Effect of initial PSD shape on wet granulation at initial 12% v/w and 1 cp viscosity: a) PSD3, b) PSD2 c) PSD1.....	28
Figure 3.7 Mass median diameter evolution in wet granulation, at 13.6% v/w and 1cp viscosity	29
Figure 3.8 Effect of binder content (1 cp viscosity) on wet granulation of coarse size powders (PSD3) with bimodal PSD: a) 9.9% v/w, b) 11.7% v/w and c) 13.6% v/w.....	32
Figure 3.9 Effect of binder content (1 cp viscosity) on wet granulation of coarse size powders (PSD3) with bimodal PSD	33
Figure 3.10 Effect of binder content (1 cp viscosity) on wet granulation of fine size powders (PSD1) with unimodal PSD: a) 9.9% v/w, b) 11.7% v/w and c) 13.6% v/w.....	34
Figure 3.11 Effect of binder content (1 cp viscosity) on wet granulation of fine size powders (PSD1) with unimodal PSD: a) 9.9% v/w, b) 11.7% v/w and c) 13.6% v/w.....	35
Figure 3.12 Change in binder content (1 cp viscosity) during wet granulation of coarse size powders (PDS3) with bimodal PSD at 9.9% v/w	36
Figure 3.13 Effect of binder viscosity on wet granulation of coarse size powders (PSD3) with initial bimodal PSD at 11.7% v/w	38
Figure 3.14 Effect of binder viscosity on wet granulation of coarse size powders (PSD3) with initial bimodal PSD at 11.7% v/w	40
Figure 3.15 Bimodal breakage, a) many small particles and a few large particles, and b) many small particles and one large particle.....	40
Figure 3.16 Effect of binder viscosity on wet granulation of fine size powders (PSD1) with initial unimodal PSD at 11.7% v/w	41

Figure 3.17 Effect of binder viscosity on wet granulation of fine size powders (PSD1) with initial unimodal PSD at 13.6% v/w: a) 1 cp, b) 2.49 cp and c) 4.85 cp.....	42
Figure 3.18 Effect of binder viscosity on wet granulation of fine size powders (PSD1) with initial unimodal PSD at 13.6% v/w: a) 1 cp, b) 2.49 cp and c) 4.85 cp.....	44
Figure 3.19 Comparison of simulations of coalescence kernels published in the literature versus the experimental data (bimodal PSD3).....	46
Figure 4.1 Schematic of aggregation of (a) equal-size particles and (b) different-size particles	51
Figure 4.2 Initial particle size distributions for wet granulation.....	57
Figure 4.3 Fitting the coalescence kernels to the experimental data of wet granulation of medium size powders (PSD3) at 13.6 %v/w of binder with 1 cp viscosity. Simulated (line) and experimental (rhombus). The end of experiment (12 minutes).....	59
Figure 4.4 Prediction of the growth kinetics of wet granulation of coarse size powders (PSD3) at 13.6 %v/w of binder with 1 cp viscosity. Simulated (line) and experimental (rhombus).....	61
Figure 4.5 Prediction of the growth kinetics of wet granulation of medium size powders (PSD2) at 13.6 %v/w of binder with 1 cp viscosity. Simulated (line) and experimental (rhombus).....	63
Figure 5.1 Granulator schematic.....	72
Figure A.0.1 Absorbance spectra for moisture calibration model of lactose-water mixture..	74
Figure A.0.2 Calibration model for lactose-water mixture.....	75
Figure A.0.3 Validation model for lactose-water mixture.....	76

1 INTRODUCTION

1.1 Justification

Wet granulation is one of the most important operations in many chemical industries including pharmaceutical, mineral processing, agricultural, chemical, and detergents. In the chemical industry, it is estimated that 60% of products are manufactured as particulates and a further 20% use powders as ingredients. The annual value of these particulates is estimated at \$1 trillion in U.S. alone [1].

In spite of its economic importance and many years of research, the understanding of the granulation process is still quite limited, and manufacturing efficiency of pharmaceutical tablets and capsules is low, rarely rises to 15 percent, and often is around 3 percent [2, 3]. The commercial interest in decreasing capital and operating costs and increasing the stability and reliability of the process has ensured that much literature has been published in the last thirty years to improve the understanding of the granulation process. Generally, this literature has focused on a qualitative understanding of the mechanisms of granule growth and the effects of different variables on granule growth behavior. However, it is still difficult to predict the granulation kinetics of a new formulation from the particle and binder initial properties such as particle size and viscosity, respectively. This is a particular problem in industries such as food, pharmaceuticals, and agricultural chemicals where there are many and frequent changes in formulations with widely varying properties.

Granulation kinetics is modeled using the population balance equation (PBE). The PBE expression of granule agglomeration on a size basis in a batch process is [4]:

$$\frac{\partial n(v)}{\partial t} = \frac{1}{2} \int_0^v \beta(v-\varepsilon, \varepsilon) \times n(v-\varepsilon) \times n(\varepsilon) \times d\varepsilon - n(v) \int_0^\infty \beta(v, \varepsilon) \times n(\varepsilon) \times d\varepsilon \quad \mathbf{1.1}$$

where $n(v)$ is the number density of particles of a specific size, t is the time, and $\beta(v, \varepsilon)$ is the coalescence kernel for agglomeration between particles of size v and ε . The difficulty in

modeling growth kinetics is focused on quantifying the coalescence kernel and to solve the PBE.

The main objective of this research is to study the effects of initial PSD shape (unimodal versus bimodal), initial particle size, and the amount and viscosity of binder on growth kinetics and the mechanism of wet granulation, and to model the agglomeration mechanism of particles from the particle and binder initial properties such as particle size and viscosity respectively. PSD was determined by means of image processing and analysis, thus, a vision system was developed and validated. Near-infrared (NIR) spectroscopy was also used, at the same time, to determine the moisture content.

1.2 Objectives

Principal

The main objective of this research is to study the effects of initial PSD shape (unimodal versus bimodal), initial particle size, and the amount and viscosity of binder on growth kinetics and the mechanism of wet granulation, and to model the agglomeration mechanism of particles, using population balance equation (PBE) and considering the initial properties of binder and particles such as viscosity and particle size, respectively.

Secondary

- Develop an algorithm to analyze gray-level images to determine particle shape and size.
- Develop and validate NIR calibration models to determine moisture content during wet granulation.
- Monitor the granule growth mechanism in a high shear mixer using vision system and NIR.
- Solve the PBE and compare the simulation results with experimental data.

2 PATTERN RECOGNITION FOR CHARACTERIZATION OF PHARMACEUTICAL POWDERS

ABSTRACT

A large part of pharmaceutical manufacturing involves the use of particulate materials. It is well known that both particle size and shape affect the physical characteristics of tablets. An image processing and analysis algorithm based on the invariant image moment technique was developed in this work to determine the particle shape by comparing features (moments) extracted from templates to those extracted from each of the objects in the image. First it determines the particle shape (rectangle, circle, etc) and then calculates its specific dimensions (diameter, aspect ratio).

The statistical validation of the vision system obtained a repeatability of 0.0012 in and 0.5% relative standard deviation and accuracy within 0.1 to 0.9% of the average value considered as true value. Also the pattern recognition technique indicated high precision and accuracy for images containing particles with some level of contact between them. The shape recognition of microcrystalline cellulose (MCC) indicated that particles of equant and acicular shape as defined by USP are predominant. The results suggest that image processing and analysis would be a suitable tool for pharmaceutical process analytical technologies (PAT) and process optimization.

2.1 Introduction

Processes involving particulates have large economic impact in many industrial fields such as pharmaceutical, food, construction, glass, and chemical. Both, the pharmaceutical and construction industries have each an annual economic impact of tens of billions of dollars [5] and in all industries an annual economic impact of a \$1 trillion is estimated in U.S. alone [1]. Despite a widespread use of particulate processes in different industries, the

techniques for particle characterization have concentrated on the determination of the size or size distribution.

However, particle size and morphology are very important in many industries. Shape and size can affect flowability and optimal conditions of particle melting and spraying in thermal spray industry [6]. In the pharmaceutical industry, it can affect flowability, compressibility, and drug delivery [7, 8].

The size of a particle or linear dimensions (side length, diameter) is related to the particle shape, for example, side length for columnar or cubical particles and diameter for spherical particles. USP requires in the General Test <776> [9] that for irregular shape particles, characterization of particle size must also include information on particle shape. At present, particle sizes of irregular particles are usually expressed as equivalent spherical diameters. The shape descriptors such as elongation, Heywood circularity, and compactness factor and concavity [10] are standard descriptors of particle's shape.

Pattern recognition is a technique frequently used in robotic systems to determine object shape. It compares the features extracted from templates to those extracted from each of the objects in the image. The traditional pattern recognition methods are normalized cross correlation, pyramidal matching, scale-invariant matching, and invariant image moments [11].

The aim of this work was to demonstrate the feasibility of using a pattern recognition algorithm based on invariant image moment [12, 13] for the determination of specific dimensions of pharmaceutical powders based on its shape, and to enhance the use of image processing and analysis as a tool within the pharmaceutical process analytical technologies (PAT) and process optimization framework. A challenge of the technique was to be able to determine the correct shape despite the contact between some of the particles.

2.2 Experimental: Samples, equipments and procedure

Spherical metal beads were used to validate the vision system in terms of size. The vision system capability to assess morphology was tested with microcrystalline cellulose and saccharose due to their wide use in the pharmaceutical and food industries, respectively.

Fig. 2.1 depicts the schematic of the vision system used to take the images of all the pharmaceutical powders and metal beads. Table 2.1 describes its components.

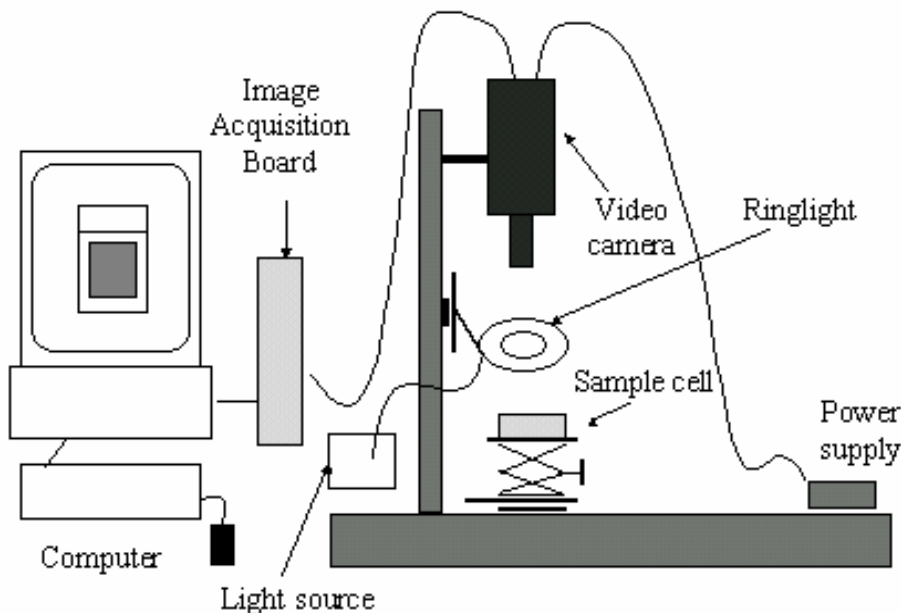


Figure 2.1 Vision System Schematic

Table 2.1 Equipments and software used to acquire and analyze images

Equipments and Software	Description
Color Image Acquisition Board	Model: IMAQ PCI-1411 (National Instruments)
Color CCD Camera	Model: GP-KR 222 (Panasonic)
Illumination System	Model: STOCKER&YALE fiber optic illuminator model 20 (quartz halogen lamp, Edmund Industrial Optics)
CCD Lens	Model: 10X CCD C-mount lens (Close focus zoom lenses, Edmund Industrial Optics)
Base Software	LabView 6i and MATLAB 6.5

An image of each pharmaceutical powder and metal beads was taken using the vision system. The images received by the color CCD camera were digitized by an image acquisition board to yield images 640×480 pixels in size. All the images were taken using the illumination system.

2.2.1 Particle Size Determination of Wet Granules

The techniques most commonly used to determine particle size of powders are sieving, image processing and analysis. The sieve method is used to measure PSD of dry powders to avoid that the wet particles stick to the vessel walls and on the mesh. A large quantity of sample is also required to obtain a reliable PSD measurement of bulk. The principal disadvantages of sieve analysis of wet granules are the agglomerate or breakage of granules during shaking [14], and low capacity to discriminate particles with little difference in size between them. On the other hand, image processing and analysis have high capacity to discriminate particles with little difference in size between them. Thus, image analysis can measure the PSD of powders recollected in a sieved section [15]. However, the sample preparation for off-line measurements of particle size is time consuming, but it is required to avoid overlapping of particles. The particle size determination of overlapped particles is currently a challenge in image processing and analysis because two or more overlapped particles could be detected as one single particle. Nevertheless, the setup of inline method could be suitable to eliminate the sample preparation and reduces the overlapping of particles. [16].

2.2.2 Experimental Design

Two experiment designs using metal beads and synthetic images were carried out to validate the vision system in order to determine shape and its size. Experimental work was also performed for morphological characterization of pharmaceutical powders. First, the experimental factorial design [17] in Fig. 2.2 was used to study the components of variability of the vision system when validating particle size determination. The algorithm based on invariant image moments was tested on a series of spherical metal beads to validate the vision system. The factors used were particle size and quantity with three levels for each factor.

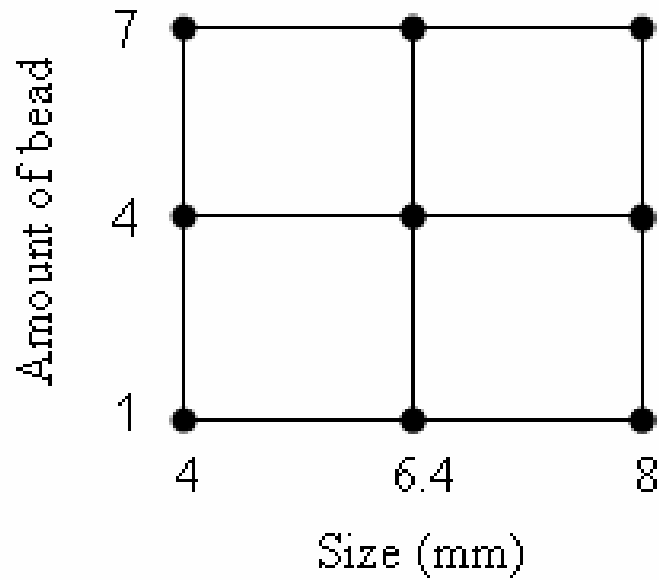


Figure 2.2 The 3^2 design for determination of the vision system capability

The experimental design to test the algorithm when used for particle shape and its size determination was carried out similarly to the method presented in [8] for comparison. Figure 2.3 depicts two synthetic images created using Adobe Photoshop 7 for the validation test. The synthetic images contain particles of different shapes, orientation, and different spatial positions. These images of acicular shape are very similar to cellulose and lactose as shown in Fig. 2.4. These images are also similar to threonine crystals, potassium glutamate, and the pharmaceutical product U2 [8].

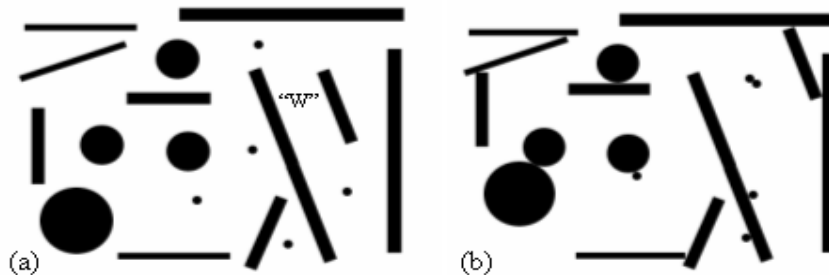


Figure 2.3 Synthetic images of different forms and sizes with particles (a) without contact and (b) in contact.

An experimental design to test the algorithm in a real application was carried out with MCC to determine the number of required particles for morphological characterization based on the equant and acicular standard shape as defined by the USP General Test <776> [9], and a 5% error of the confidence interval. Two equant templates including circle and square and four acicular templates of different aspect ratio were used for morphological characterization.

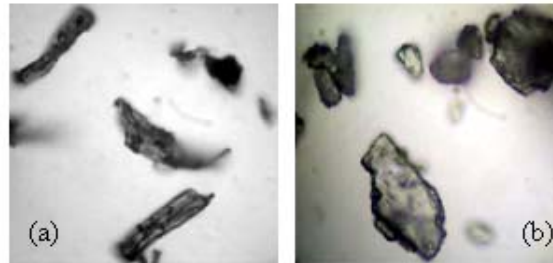


Figure 2.4 Real shape of (a) Microcrystalline cellulose and (b) lactose monohydrate

2.3 Image processing and analysis

Figure 2.5 depicts the algorithm for image processing and analysis using pattern recognition. As mentioned before, first, images of 640×480 pixels in size were taken by the CCD camera. A smoothing treatment with a linear filter was performed to reduce the noise. The filtering replaces each pixel by a weighted sum of its neighbors [18]. If $P(i,j)$ represents the intensity of pixel P with coordinates (i, j) , the pixels surrounding $P(i,j)$ can be indexed as follow (for a 3×3 matrix):

$P(i-1, j-1)$	$P(i, j-1)$	$P(i+1, j-1)$
$P(i-1, j)$	$P(i, j)$	$P(i+1, j)$
$P(i-1, j+1)$	$P(i, j+1)$	$P(i+1, j+1)$

A smoothing linear filter assigns to $P(i, j)$ a value that is a linear combination of its surrounding values. For example, the new value of gray-level of pixel $P(i, j)$ is:

$$P(i, j)_{new} = \left\{ \sum_{m=-1}^1 \sum_{n=-1}^1 P(i+m, j+n) \right\} / 9 \quad 2.1$$

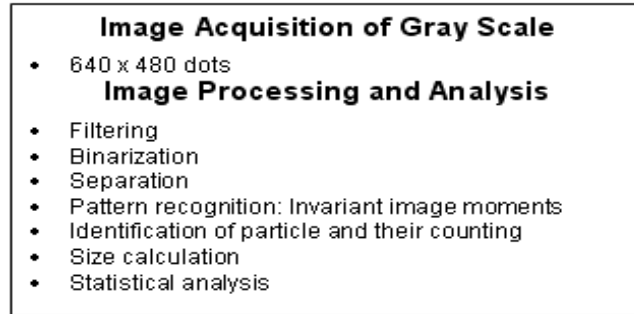


Figure 2.5 Schematic flow of algorithm for image processing and analysis.

Next, a binarization procedure was performed to transform the gray image to a binary one establishing a threshold based on the histogram of gray-level values. After binarization, some overlapped particles could be detected as a large single binary particle. A technique for separation of particles using erosion and dilation processes is automatically applied to decrease this problem. A layer of pixels was removed and added using a 3×3 structuring element for erosion and dilation techniques, respectively. Finally, the particle shape using the technique of invariant moments is determined as described below.

Invariant Moments

Image moments have attracted great attention in pattern recognition due to their mathematical simplicity and numerous physical interpretations of an image. The interpretation of the first three moments is area, centre of mass, and inertia of an image. The two-dimensional moments of order (p+q) of an image $f(x,y)$ are defined by

$$m_{pq} = \int_{-\infty}^{\infty} \int_{-\infty}^{\infty} x^p y^q f(x, y) dx dy \quad \text{for } p, q = 0, 1, 2, \dots \quad 2.2$$

where f is the brightness or gray scale (between 0 and 255) of the point (x, y) where x and y represent the spatial coordinates of a picture element (pixel). For this, the image must be represented as a matrix where each element is a pixel with a gray level value.

Hu [12, 13] extended the application of image moments to pattern recognition. Additional studies [19, 20, 21] demonstrate other applications of image moments in image processing and analysis, too. Hu [12, 13] derived relative and absolute combinations of central moments that are invariant with respect to scale, position, and orientation and thus each shape is characterized by a unique set of values of the invariant moments. The two-dimensional central moments of order $(p+q)$ of an image $f(x,y)$ are defined by

$$\mu_{pq} = \int_{-\infty}^{\infty} \int_{-\infty}^{\infty} (x - \bar{x})^p (y - \bar{y})^q f(x, y) dx dy \quad \text{for } p, q = 0, 1, 2, \dots \quad 3.3$$

where

$$\bar{x} = \frac{m_{10}}{m_{00}}; \bar{y} = \frac{m_{01}}{m_{00}} \quad 3.4$$

These central moments were used by Hu [12, 13] to define seven functions based on the central moments up to order three that are invariant with respect to object scale, translation, and rotation.

$$\phi_1 = \mu_{20} + \mu_{02} \quad 3.5$$

$$\phi_2 = (\mu_{20} - \mu_{02})^2 + 4\mu_{11}^2 \quad 3.6$$

$$\phi_3 = (\mu_{30} - 3\mu_{12})^2 + (3\mu_{21} - \mu_{03})^2 \quad 3.7$$

$$\phi_4 = (\mu_{30} - \mu_{12})^2 + (\mu_{21} - \mu_{03})^2 \quad 3.8$$

$$\phi_5 = (\mu_{30} - 3\mu_{12})(\mu_{30} + \mu_{12})[(\mu_{30} + \mu_{12})^2 - 3(\mu_{21} + \mu_{03})^2] \\ + (3\mu_{21} - \mu_{03})(\mu_{21} + \mu_{03})[3(\mu_{30} + \mu_{12})^2 - (\mu_{21} + \mu_{03})^2] \quad 3.9$$

$$\phi_6 = (\mu_{20} - \mu_{02})[(\mu_{30} + \mu_{12})^2 - (\mu_{21} + \mu_{03})^2] \\ + 4\mu_{11}(\mu_{30} + \mu_{12})(\mu_{21} + \mu_{03}) \quad 3.10$$

$$\phi_7 = (3\mu_{21} - \mu_{03})(\mu_{30} + \mu_{12})[(\mu_{30} + \mu_{12})^2 - 3(\mu_{21} + \mu_{03})^2] \\ - (\mu_{30} - 3\mu_{12})(\mu_{21} + \mu_{03})[3(\mu_{30} + \mu_{12})^2 - (\mu_{21} + \mu_{03})^2] \quad 3.11$$

By computing the seven functions (invariant image moments) for each particle or object in the image and comparing the set to those for the templates or reference images, a particular shape can be assigned to each particle in the image with a certain level of tolerance.

2.4 Results and discussion

2.4.1 Statistical validation in determining particle size using spherical shape

The repeatability obtained from variance analysis with the experimental design shown in Fig. 2.2 was 0.0011 in. This experimental design is a common industrial application called gauge capability studies [17]. Table 2.2 includes also the results of repeatability carried out as per the guideline of FDA [22], to characterize the vision system and a commercial caliper. The repeatability obtained for the vision system was 0.0012 in and an accuracy within 0.1 to 0.9 % of the true value. The reference method used was a caliper with repeatability reported by the manufacturer of 0.0005 in and an experimental repeatability of 0.0007 in. Commercial calipers considered as excellent have repeatability of 0.001 in.

Table 2.2 Study of repeatability of metal bead.

Caliper Diameter (inch)	Vision System Diameter (inch)
0.2516	0.2551
0.2516	0.2555
0.2512	0.2535
0.2508	0.2555
0.2531	0.2559
0.2512	0.2575
0.2512	0.2563
0.2520	0.2563
Mean: 0.2516	Mean: 0.2557
SD ^a : 0.0007	SD: 0.0012
RSD ^b : 0.2822 %	RSD: 0.4501 %

^{a, b} Standard deviation and relative standard deviation, respectively.

2.4.2 Statistical validation of pattern recognition technique for determination of shape and its size

The shape recognition algorithm based on invariant moments was tested similarly to the test established by Pons et al. [8]. Initially, it was tested with synthetic images (Fig. 2.3a) containing particles without any contact between them. Table 2.3 compares estimated values by the vision system to the true ones. As can be seen the precision and accuracy decrease as the size (from length to breadth) decreases. They also decrease as the particle angle with respect to the horizontal or vertical increases from 0 to 45 degrees. This effect is observed in acicular inclined particles as shown by the particle "w" in Fig. 2.3a and in circular particles.

The diminution in repeatability and accuracy observed is due to the discrete form of the images (640×480 dots). This observation agrees with results obtained by other authors [8].

Table 2.3 Study of repeatability for images with particles without contact

	Average	Standard deviation	R.S.D.
L / l	1.00	0.02	1.78 %
B / b	1.02	0.06	6.20 %
D / d	0.90	0.06	6.86 %

R.S.D.= relative standard deviation

In Table 2.3, L is the real length, l is the estimated length, B is the real breadth, b is estimated breadth, D is the real diameter, and d is the estimated diameter.

Images containing particles with some level of contact between them, similar to the highest level (S7) defined by Pons et al. [8], were created as shown in Fig. 2.3b. The algorithm, based on invariant moments, again separates and classifies correctly the different particles as shown in Fig. 2.6, and both, the precision and accuracy for particles in contact (as shown in Table 2.4) are similar to those of the acicular and equant particles without contact in Fig. 2.3a.

However, it is observed that the precision and accuracy decrease for particles in contact as compared to particles without contact, as indicated by relative standard deviations (R.S.D.) in Tables 2.3 and 2.4.

Table 2.4 Study of repeatability for images with particles in contact

	Average	Standard deviation	R.S.D.
L / l	1.00	0.02	1.66 %
B / b	1.02	0.07	6.42 %
D / d	0.89	0.07	8.04 %

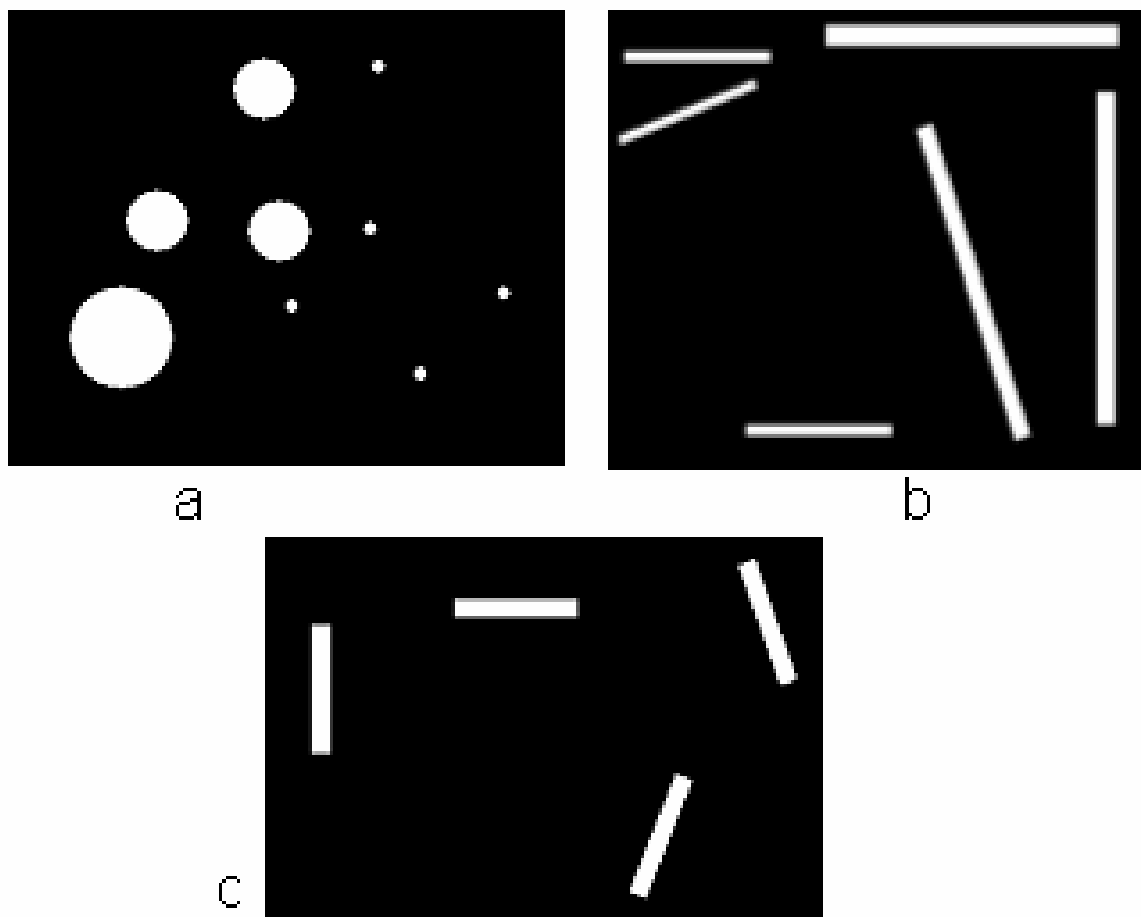


Figure 2.6 Synthetic images separated and classified (a) circular particles (c) acicular particle with $R=10$ (d) acicular particles with $R=5$ ($R=length/breadth$)

The pattern recognition algorithm was also tested with MCC and saccharose. Figure 2.7 depicts the image processing steps, where the binarization step (Fig. 2.7b,f) indicates particles in contact. Then an erosion and dilation process as indicated in Fig. 2.7c,g and Fig.

2.7d,h respectively was applied to separate particles with some contact level, similar to the highest level (S7) defined by Pons et al. [8]. The particles were then characterized as explained in next section. The algorithm works with real as well as synthetic particles and without any tuning required.

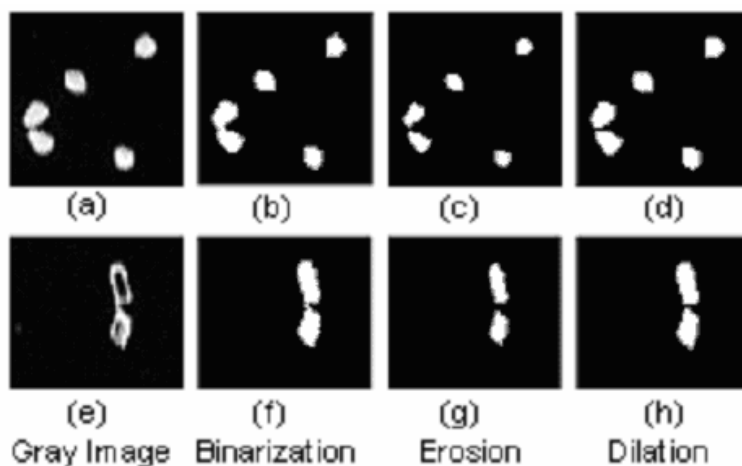


Figure 2.7 Image Processing steps for (a) microcrystalline cellulose and (e) sucrose

2.4.3 Morphological characterization of pharmaceutical powders

First, six templates of equant (circle and square) and acicular shape as defined by the USP General Test [9] were created. Different aspect ratios ($R = \text{length}/\text{width}$) were created for the acicular shape. These shapes are common in many pharmaceutical powders [8, 23] such as microcrystalline cellulose, lactose monohydrate, salicylic acid, sucrose, threonine, and potassium glutamate, see Fig. 2.4.

Next, the total number of particles necessary to reliably classify morphologically the MCC was determined based on the number of particles necessary to achieve a 5% error of the confidence interval for each template using Eq. 3.12.

$$n = \left(\frac{S \times t}{k \times x} \right)^2 \quad 3.12$$

where n is the number of particles, S is the standard deviation, t is the statistic t , k is the error and \bar{x} is the average.

The number of required particles for each shape template was confirmed by considering the change of the template standard deviation versus number of particles (Fig. 2.8). The number of particles for each six templates was about 80 similar to Pons' results. Based on the natural shape composition of the MCC, the total number of particles necessary to assess MCC morphology and its size is approximately 2000 to have 80 particles of the shape in less presence.

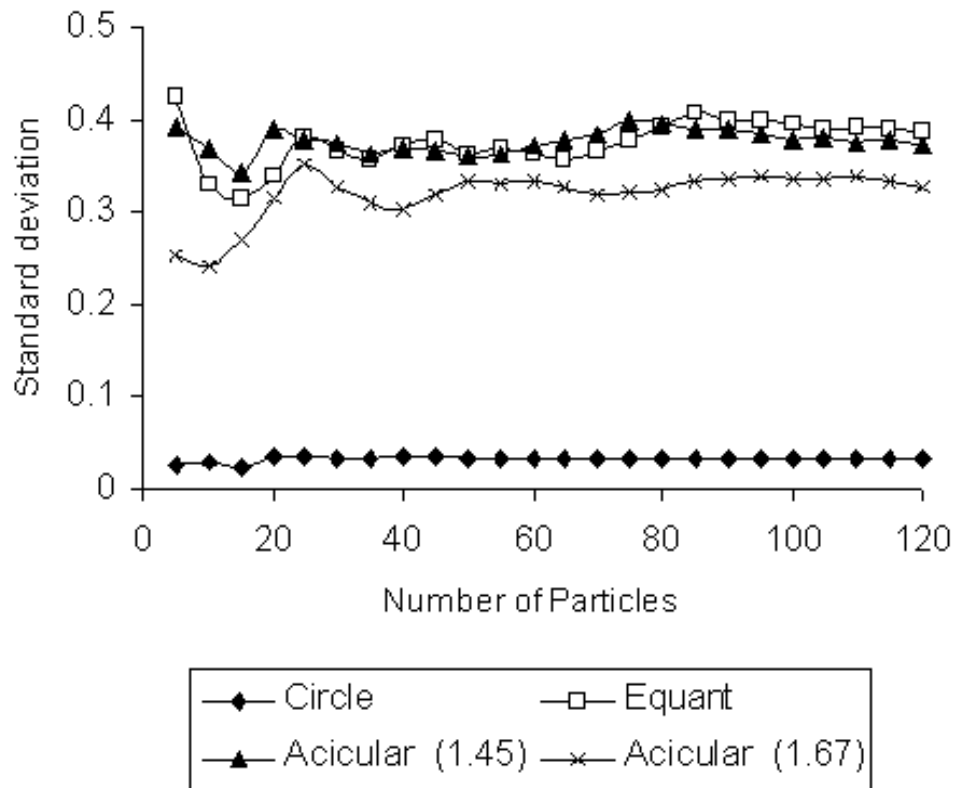


Figure 2.8 Change of standard deviation of each template versus number of particles

A set of 18 images (1984 particles) were analyzed to determine particle shape where 23.2% of the particles were classified as square, 21.1% as circle, 29.6% as acicular, and 26.1% of the particles were classified as other (no standard shape). The level of tolerance to classify the particles in terms of shape was 88%.

The time required to analyze the 18 images (an average number of 111 particles per image) was approximately 22 seconds. The speed of analysis and accuracy in the prediction, poses this algorithm as a suitable tool to monitor inline the granule size distribution and shape, for example, in a fluidized bed granulation system, Watano and Miyanami [16].

2.5 Conclusions

The technique of invariant image moments is suitable for the characterization of pharmaceutical powders in terms of morphology and size. The algorithm allows identification and measurement of particles according to its shape. The vision system yielded high precision and accuracy in identifying and measuring particles, despite the contact among themselves. The precision and accuracy decrease however as the particle angle with respect to the horizontal or vertical increases from 0 to 45 degrees and as the particle size decreases. These effects could be reduced by increasing the resolution of discrete images.

The morphological characterization of MCC indicates high quantity of particles of the equant and acicular shape as defined by USP. The minimum number of particles for each shape was about 80 and the total number of particles necessary to assess morphology and its size was 1984 (18 images). The time required to analyze a set of 18 images was about 22 sec. This rapid analysis of the images makes the algorithm of image processing and analysis a suitable tool for inline pharmaceutical process analytical technologies (PAT). The technique can be expanded by adding new templates and its corresponding set of the seven invariant moments.

3 EFFECT OF PARTICLE AND BINDER CHARACTERISTICS ON THE GROWTH KINETICS AND MECHANISM OF WET GRANULATION

ABSTRACT

The effect of initial particle size and initial distribution shape, unimodal versus bimodal, and binder characteristics on the growth kinetics and mechanism of wet granulation were evaluated. Wet granulation of pharmaceutical powders with initial bimodal particle size distribution (PSD) presented growth kinetics consisting of two stages: a fast growth followed by a slow growth. Fast stage is controlled by binder amount and the high probability of coalescence due to the collisions of small and large particles. The second stage is characterized by slow agglomeration of powder mixtures with water content 13.6% v/w, and slow breakage of powder mixtures with water content of 9.9 and 11.7% v/w. Wet granulation of pharmaceutical powders with initial unimodal PSD exhibited slow growth kinetics consisting of one stage. Similar particle size did not promote the agglomeration.

The binder viscosity has opposite effect in each stage of wet granulation of powders with initial bimodal PSD, at 11.7% v/w of binder or lower. The growth rate increases with an increase in binder viscosity during the first stage, while the growth rate decreases with increase in binder viscosity during the second stage. In general, the variations in the three factors are consistent with the *viscous Stokes' (St_v) number*. The probability of a successful collision increased with smaller particle size, higher binder viscosity, and higher binder content.

3.1 Introduction

Wet granulation in a high shear mixer is primarily a process for particle enlargement that is used in many industries such as pharmaceutical, mineral processing, agriculture, food, and detergent. The process of particle enlargement via a coalescence mechanism improves the

flow properties of the particles, and decrease segregation of the ingredients, thus also improving the uniformity of the mixture [24]. A granule breakage mechanism could also happen during the wet granulation process, depending upon the viscosity and the amount of binder.

Ennis *et al.* [25] developed a *viscous Stokes' (St_v) number*, wherein factors such as particle size and density, and binder viscosity and amount are considered to quantify the probability of particle coalescence and, as a consequence, the granule growth rate. Ennis *et al.* [25, 26] considered the viscosity force of a liquid bridge, and modeled two colliding granules using the equation of motion (3.1):

$$m_p \frac{dv}{dt} = \frac{3\pi \mu r_p^2}{2x} v \quad 3.1$$

where m_p is the granule's mass; v is the relative velocity between the two particles; r_p is the granule's radius; μ is the viscosity of the binder liquid and $2x$ is the distance between colliding granules. The analytical solution of Eq. 3.1 is

$$v = v_0 \left[1 - \frac{1}{St_v} \ln \left(\frac{h_0}{x} \right) \right] \quad 3.2$$

where h_0 is the thickness of the liquid layer on the surface of the particle and St_v is the viscous Stokes number given by

$$St_v = \frac{8\rho_p v_0 r_p}{9\mu} \quad 3.3$$

where ρ_p is the particle density. The particles will coalesce upon collision, if the viscous Stokes number of the particles is smaller than a critical value of the viscous Stokes' number (St_v^*), given by:

$$St_v^* = \left(1 + \frac{1}{e} \right) \ln \left(\frac{h_0}{h_a} \right) \quad 3.4$$

where e is the coefficient of restitution based upon linear velocity differences of the particles before and after impact; and h_a represents the characteristic length of the surface asperities.

Recently, the importance of Ennis' theory has inspired researchers [14, 27, 28, 29] to further study the effects of particle size, binder viscosity and amount on the growth kinetics and mechanism of wet granulation. For instance, Mill *et al.* [27] found that the growth rate of sand in a low shear mixer increases with an increase in the amount of a low viscosity binder (up to maximum 100 mPa s), such as silicone. They also found that the growth rate decreases with increase in the amount of binder with a viscosity higher than 100 mPa s.

Badawy and Hussain [29] determined in experiments with anhydrous lactose that the growth rate increases with a decrease in initial particle size, in accordance with Ennis' theory, wherein smaller particles present low kinetic energy that is dissipated easily in the binder layer. Ennis *et al.* [25] and Adetayo *et al.* [28] observed a sequential two-stage mechanism during the wet granulation of fertilizers with a wide size distribution, while Mills *et al.* [27] failed to observe the sequential two-stage mechanism during the granulation of materials with a narrow size distribution.

Powders with bimodal PSD or wide size distribution have many small and large particles that favor the preferential coalescence between small and large particles, as suggested by Tardos *et al.* [30] with their layering mechanism or coalescence of coarse and fine particles (Figure 3.1). Hounslow *et al.* [31], and Boerefijn and Hounslow [32] also developed size-dependent agglomeration kernels that mathematically favored the coalescence of small and large particles. On the contrary, it is believed that powders with unimodal PSD or narrow size distribution have similar size particles which do not favor the preferential coalescence between small and large particles. However, the effect of initial PSD shape (unimodal PSD or narrow size distribution and bimodal PSD or wide size distribution) on mechanism and growth kinetics of wet granulation has not been studied appropriately to increase the fundamental understanding of particle agglomeration mechanism.

The main objective of the current work is to study the effects of initial PSD shape (unimodal versus bimodal), initial particle size, and the amount and viscosity of binder on growth kinetics and the mechanism of wet granulation. Particle size distribution (PSD) was

determined by means of image processing and analysis [33]. Near-infrared (NIR) spectroscopy was used, at the same time, to determine moisture content.

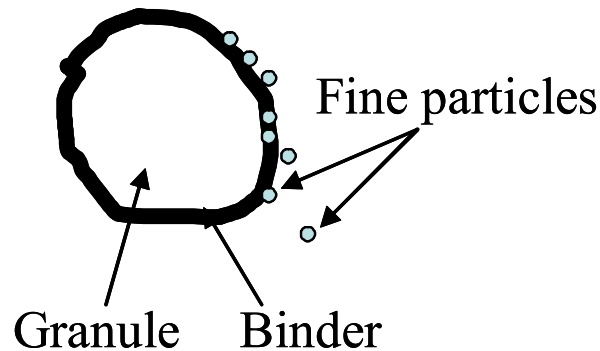


Figure 3.1 Layering growth mechanism proposed by Tardos et al. (1997)

3.2 Experimental Methods

3.2.1 Materials and equipments

Pharmaceutical powders such as lactose anhydrous supplied by Sheffield Products and lactose monohydrate manufactured by *FOREMOST FARMS USA #55-0072* and supplied by *Mutchler Inc.* (Cayey, PR), were used in the experiments of wet granulation. Figure 3.2 shows the three particle size distributions used in the wet granulation experiments, designated as PSD1 (fine size powders), PSD2 (medium-size powders) and PSD3 (coarse size powders).

The three levels of particle size were prepared by screening lactose monohydrate and anhydride using the following sieve trays Tyler's 270, 230, 200, 170, 140, 70, 50 and 40 mesh US Standard. The PSD of powders recollected in each sieve tray was measured (PSD1, PSD2 and PSD3) by means of image processing and analysis [33].

A viscometer was used to measure the viscosity of Povidone-water mixtures at room temperature. Three levels of Povidone-water mixture (0%, 5% and 9% of Povidone) were

prepared to obtain homogeneous binder solutions with viscosities of 1, 2.49 and 4.85 cp at room temperature. The Povidone was manufactured by ISP Technologies INC.

A viscometer was used to measure the viscosity of Povidone-water mixtures at room temperature. Three different amounts of solid Povidone (0%, 5% and 9%) were dissolved in water at room temperature to obtain homogeneous binder solutions with viscosities of 1, 2.49 and 4.85 cp, respectively. The Povidone was manufactured by ISP Technologies INC.

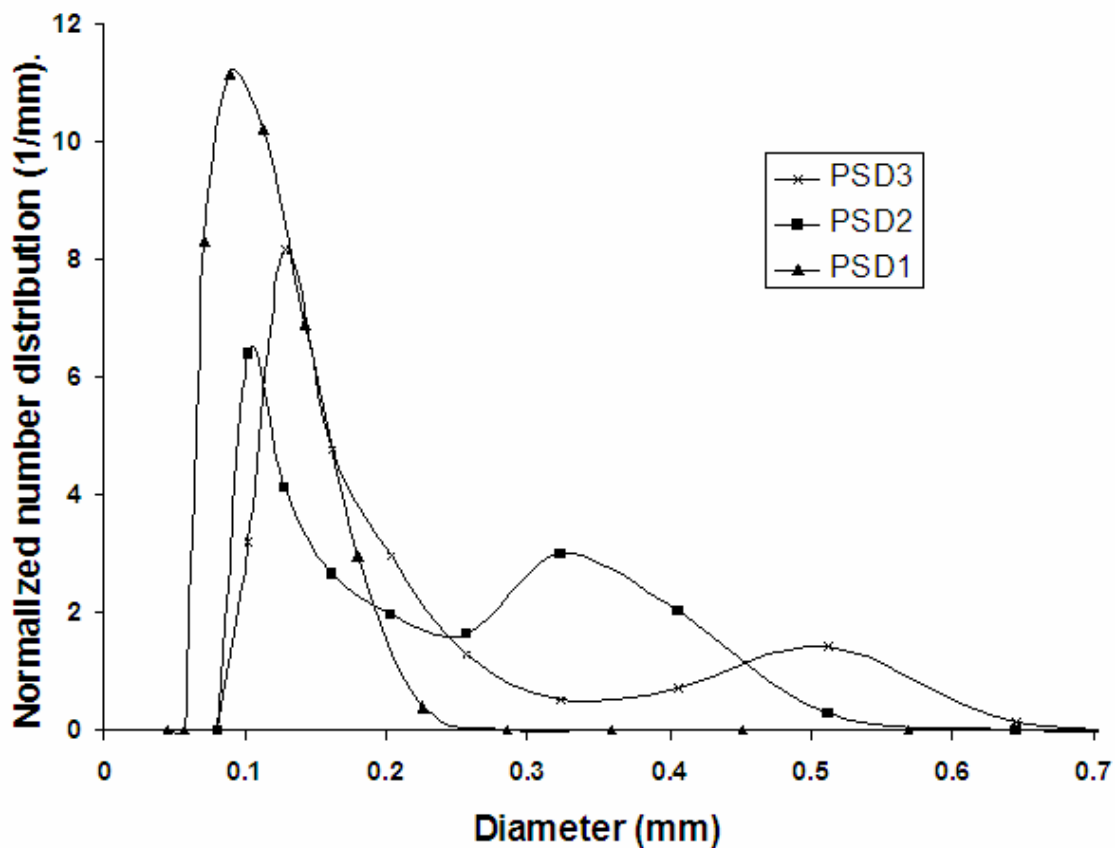


Figure 3.2 Initial particle size distributions for wet granulation

Figure 3.3 depicts a scheme of a laboratory-scale high shear mixer equipped with an NIR spectrometer. A Ryobi™ 12-inch drill press was used as an impeller motor, rotating vertically; its speed was fixed at 560 rpm. Two stainless steel blades were attached to the

impeller axis. The liquid binder was added to the powder mixture at a rate of 161.7 ml/min by means of a peristaltic pump through a nozzle.

Although this is a laboratory-scale high shear mixer, the down-scaling of the wet granulation process allows an acceptable-mixed process without a significant spatial variation in PSD and, therefore, to obtain reliable measurements. The spatial variation of PSD (or PSD uniformity) in a granulator is modeled by the term $(\nabla \cdot (v n))$ of the population balance equation [4] (see Eqs. 3.5 and 3.6).



a)



b)

Figure 3.3 Laboratory-scale high shear mixer

$$\frac{\partial n}{\partial t} + \nabla \cdot (v n) - B + D = \frac{1}{V} (\sum Q_{in} \times n_{in} - \sum Q \times n) \quad 3.5$$

$$\nabla \cdot (v n) = \frac{\partial (v_x n)}{\partial x} + \frac{\partial (v_y n)}{\partial y} + \frac{\partial (v_z n)}{\partial z} \quad 3.6$$

where n is the number density function; t is the time; G is the growth rate; l is a length of the particle; v is particle velocity; B and D are the birth and death rate, respectively; V is the mixer volume; and Q_{in} and Q are the flow rates.

In order to obtain an acceptable mixing quality, the zone of poor mixing in the granulator located near the vessel wall and in the vessel bottom had to be reduced. This was achieved by reducing the space between the blades and the vessel wall, and by positioning the blades equidistantly in the vessel as shown in Figure 3.3b.

3.2.2 Granulator Characterization

The granulator was tested to determine the spatial variation of PSD and, therefore, the experiment reproducibility. Four samples were taken in four different zones of the granulator (Figure 3.4), and analyzed by means of image processing and analysis [33] to determine the PSD. Figure 3.5 shows a similar cumulative mass percentage for the two zones of the mixer, top and bottom. Furthermore, the low standard deviation for mass median diameter (Table 3.1) indicates similar granule size measurements in four positions inside the mixer. Mass median diameter is the diameter in which exactly one-half of the mass is conformed by smaller particles, than mass median diameter, and the other half of the mass is conformed by larger particles.

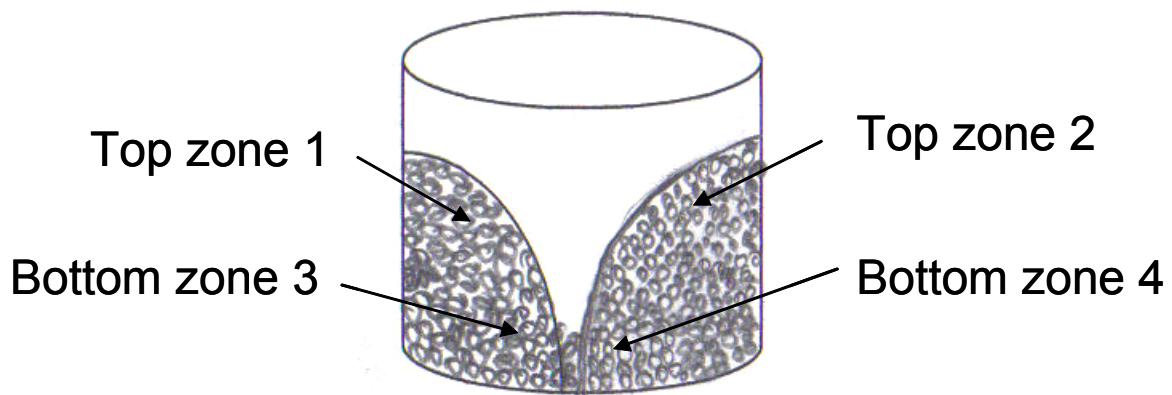


Figure 3.4 Zones inside the granulator

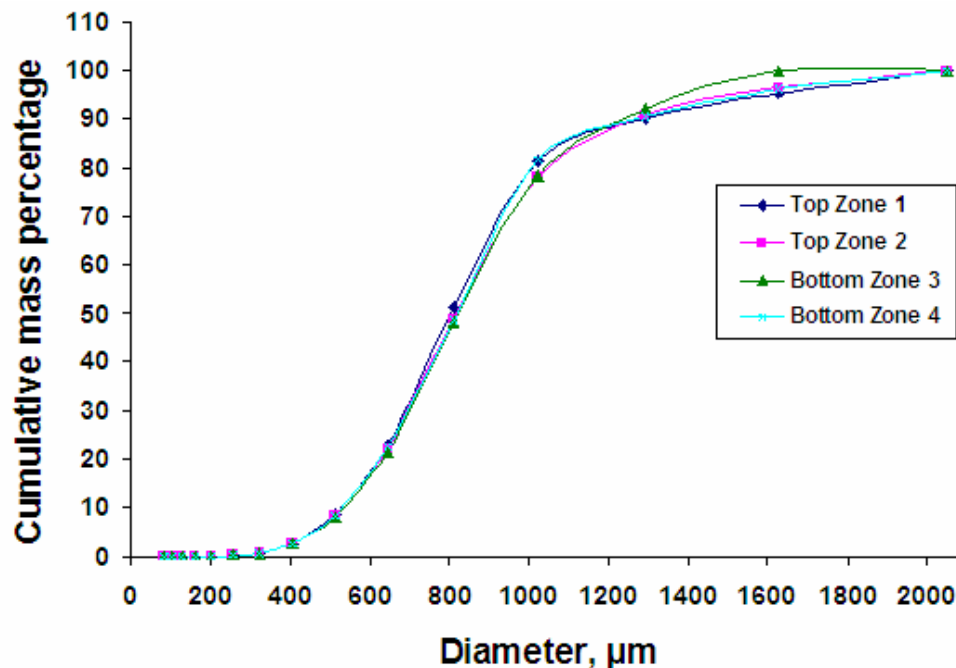


Figure 3.5 Cumulative mass percentages for the four different zones inside the granulator

Table 3.1 Study of repeatability

Vessel zones	Mass median diameter, [μm]
Top zone 1	808
Top zone 2	820
Bottom zone 3	823
Bottom zone 4	821
Mean	818 μm
S.D.	6.78 μm
R.S.D.	0.83%

S.D= standard deviation; R.S.D.= relative standard deviation

3.2.3 Granulation Process

Approximately 90 g of lactose monohydrate and 345 g of lactose anhydride were mixed during five minutes in a high shear mixer, operating at 560 rpm. Homogenization of the powder mixture is ensured using an NIR spectrometer, the dry powders were mixed until the spectrum did not change significantly with respect to the previous one. Water was then added

to the lactose mixture by means of a peristaltic pump through a nozzle and the powder mixture was granulated. The granulator was stopped after the first minute to extract samples from different points inside the mixer to measure PSD, and to collect off-line spectra. This experimental procedure was repeated at 2, 4, 6, 8, 10 and 12 minutes.

3.2.4 Experimental Design

The experiments to study wet granulation behavior using lactose anhydrous and monohydrate were carried out following the Split-Plot experimental design [17], consisting of three factors and three levels for each factor, plus two replicates, as shown in Table 3.2. The Split-Plot design consists of factorial experiments, not completely randomized.

Table 3.2 Experimental Design

Factors	Particle size distribution (mm). Figure 2.1			Binder viscosity (cp)			Amount of binder (% V _{Liquid} /W _{Solid})		
	PSD1	PSD2	PSD3	1	2.49	4.85	9.9	11.7	13.6
Levels									

3.3 Development of the Calibration Model for Moisture Content Determination

The calibration model to determine the moisture content of the powder mixture was developed using NIR spectroscopy and LOD data. The collection and transformation of spectral data were performed using spectroscopic analysis software (OPUS). For quantitative analysis of the moisture content of the powder mixture, NIR spectroscopy spectra required a multivariate calibration model. The calibration procedure involved collecting a number of samples, obtaining for each sample both the moisture content using the reference method (LOD) and the absorbance value using NIR spectroscopy. A multivariate calibration model was developed from these data, by means of partial least squares (PLS) [34, 35, 36]. The calibration model was used to predict moisture content in future samples. Absorbance spectra for calibration model are presented in Appendix A.

3.4 Results and Discussion

3.4.1 *Effect of initial PSD shape (unimodal versus bimodal) on the mechanism and growth rate of wet granulation*

The normalized number distribution was used to show the change in PSD over time, as indicated in Figure 3.6. The two-stage coalescence mechanism was observed in the wet granulation of pharmaceutical powders at 12% of binder with both initial unimodal and bimodal PSD. The bimodal PSD showed a fast growth followed by a slow one while the unimodal PSD showed an opposite mechanism, slow growth followed by a fast one as can be observed in Figure 3.5 through the evolution of mass median diameter of particles during granulation.

The initial bimodal PSD (Figure 3.6a and 3.6b) exhibits first a fast stage of granule growth. This stage is controlled by both, the binder amount added during the first 30 seconds and the high probability of collision between small and large particles that increases the growth rate. The opposite case is observed with initial mono-dispersed unimodal PSD (Figure 3.6c). The first stage of granule growth is slow, due to the high concentration of particles of similar size, which does not favor coalescence mechanism. Enlargement of the particles occurs over the first six minutes of wet granulation. This enlargement of particles transforms the distribution shape from mono-dispersed unimodal PSD to poly-dispersed unimodal PSD, with a volume ratio of small to large particles of approximately 150. This volume ratio is similar to the volume ratio observed with bimodal PSD. This change to poly-dispersed unimodal caused the second stage to be fast, similar to bimodal distribution which is controlled by the high probability of collision between small and large particles.

The strength of the liquid bridge between particles of similar sizes is weaker than between small and large particles due to the force exerted downwards by the weights of each particle. The higher strength of the liquid bridge between small and large particles, and lower kinetic energy of small particle, allows the particles to stay in contact long and, thus, the small particle will join the larger one by diffusion of small particle through binder layers. The

preferential coalescence between small and large particles is supported by a layering mechanism or coalescence of coarse and fine particles (Figure 3.1) described by the Stokes' number if sizes between colliding particles are different [30], and by size-dependent agglomeration kernels developed by Hounslow et al. [31], and Boerefijn and Hounslow [32].

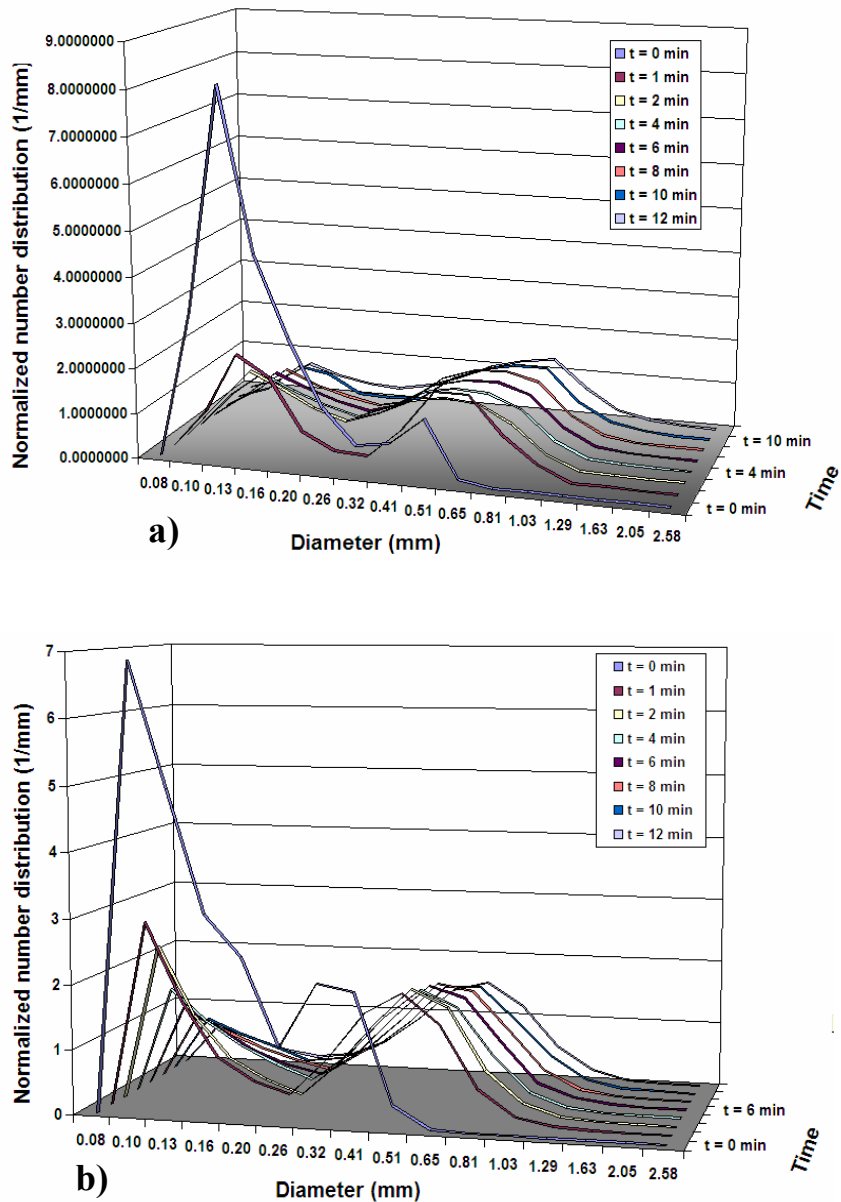


Figure 3.6 Effect of initial PSD shape on wet granulation at initial 12% v/w and 1 cp viscosity: a) PSD3, b) PSD2 c) PSD1

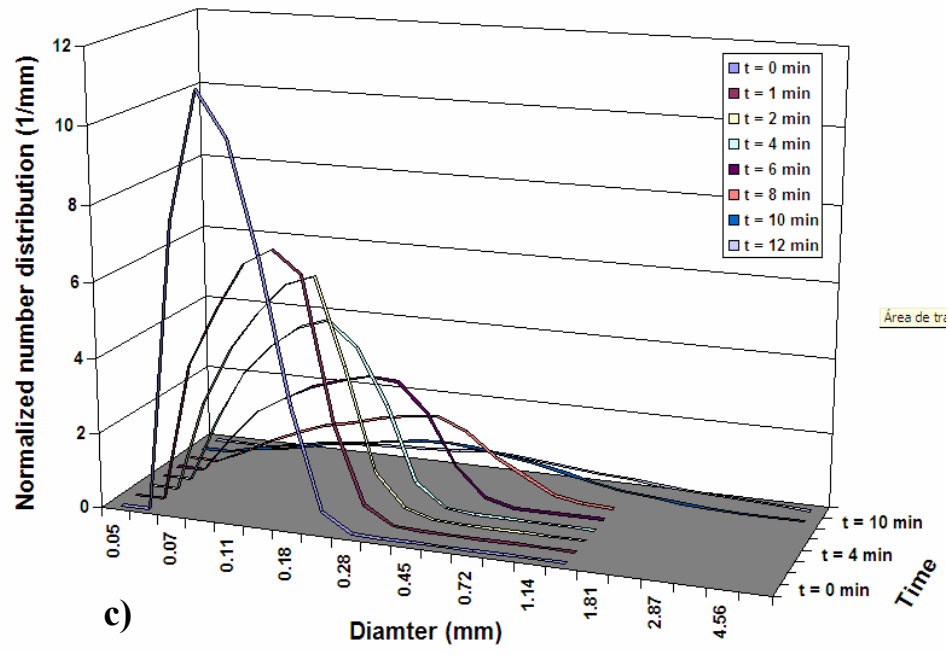


Figure 3.6 (continued)

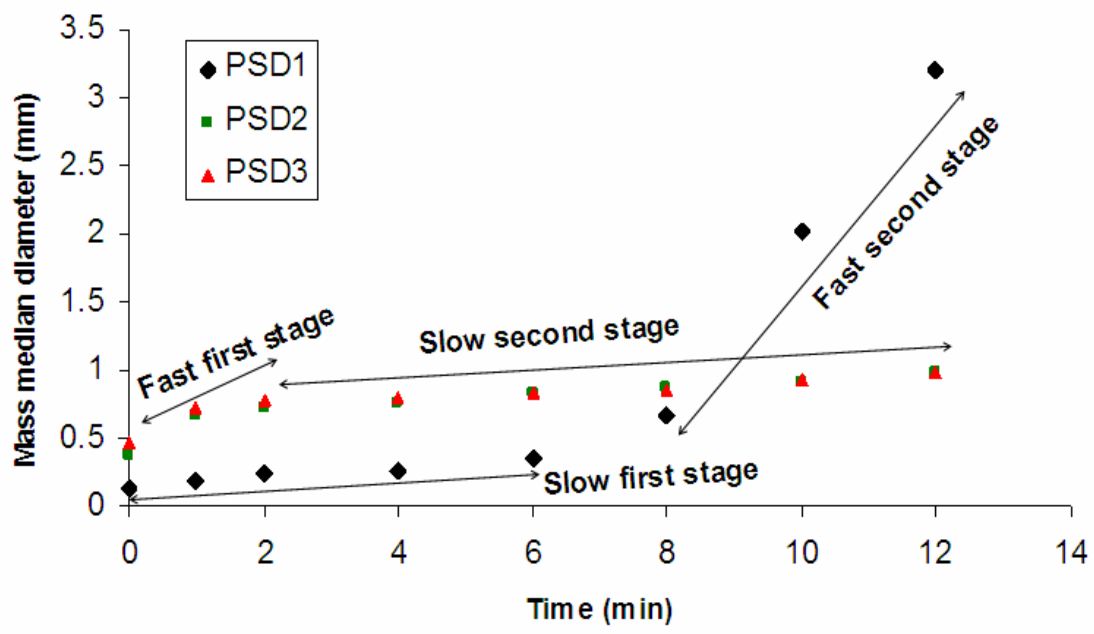


Figure 3.7 Mass median diameter evolution in wet granulation, at 13.6% v/w and 1cp viscosity

The gradient of each line in Figure 3.7 is shown in Table 3.3, and represents the granule growth rate, similar to that calculated by Mills *et al.* [27]. For wet granulation of powders with initial bimodal PSD, the growth rate increases with decrease in particle size, as indicated in Table 3.3. These results are consistent with Ennis' theory [25].

Table 3.3 Effect of particle size on granule growth rate at 13.6% v/w and 1cp viscosity

Mass media Diameter (mm)	PSD	Stage	Growth Rate (mm/min)	Ratio: fast/low
0.46	PSD3: bimodal	First: fast	0.160	8.0
		Second: slow	0.020	
0.37	PSD2: bimodal	First: fast	0.175	6.7
		Second: slow	0.026	
0.13	PSD1: unimodal	First: slow	0.038	16.7
		Second: fast	0.634	

3.4.2 Effect of Initial Particle Size on Granule Growth Rate in Wet Granulation

Figure 3.7 shows how mass median diameter increased over time for all the three size ranges of powders (PSD1, PSD2, and PSD3), at 13.6% v/w and 1cp viscosity. The figure depicts again that particle growth rate increases with a decrease in initial particle size, as indicated by the mass median diameter in Table 3.3. Using Fig. 3.7 and Table 3.3, it can be demonstrated that fine powders with initial unimodal PSD exhibit a faster growth rate in the second stage of wet granulation than the growth rate observed in the first stage of wet granulation with medium-sized and coarse powders. This phenomenon occurs due to a mono-dispersed unimodal PSD becoming a poly-dispersed unimodal PSD over the first six minutes, favoring agglomeration of particles.

However, for fine powders with initial unimodal PSD at 9.9 and 11.7% v/w, the stage of rapid growth rate was not evident during wet granulation. Instead, a one-stage mechanism of slow granule growth rate was predominant. A slow growth rate at low binder content is due to the high cohesive force of small particle produced by the large contact surface, leading to

strong granules that the material, in itself, is hard to deform, thereby decreasing agglomeration. The addition of liquid makes the agglomerate more deformable due to decreased particle-particle interactions. These results are in accordance with results reported by Jægerskou *et al.* [37], that ball growth may occur if too much liquid is added, or if granulation times are too long.

3.4.3 *Effect of binder content on granule growth and the mechanism of wet granulation*

Figures 3.8 and 3.9 depict the effect of binder amount on the growth of the particles. A change in the binder amount can alter the mechanism and growth rate in the second stage of wet granulation. For powders with initial bimodal PSD, the mechanism changes from a particle agglomeration at 13.6% v/w of binder, to a particle breakage mechanism at 9.9 and 11.7% v/w of binder. For powder mixtures with initial unimodal PSD, the variation in binder amount can also change the number of stages from two (slow and fast) at 13.6% v/w of initial binder, to one for 9.9 and 11.7% v/w of initial binder, as observed in Figures 3.10 and 3.11.

The initial fast growth is maintained by high liquid content added during the first 30 seconds and by the high probability of collisions between small and large particles, these collisions facilitate coalescence. The second stage is characterized by a slow breakage mechanism, due to the low moisture content (9.9 and 11.7% v/w) and binder evaporation (Figure 3.12) induced by the high shear force that does not prevent the particle breakage, and by slow agglomeration of particles, due to the decreasing size difference between particles.

There is a minimum critical value of liquid content on the granule surface that will trigger the second stage of slow growth rate to proceed. This minimum value of liquid content is required to form a liquid layer on granule surface to increase the coalescence probability between particles. Above this critical minimum value, there is a high probability of only one stage of fast growth. The end of the first stage of fast granule growth is related to the end of binder addition, and the beginning of the slow granule growth or breakage without

a significant change of particle size. These observations are consistent with results obtained by Holm et al. [38,], Lindberg [39], Schaefer et al. [40] and Mackaplow et al. [14]. Although, the fast granule growth can continue if too much initial liquid is added (Figure 3.8c).

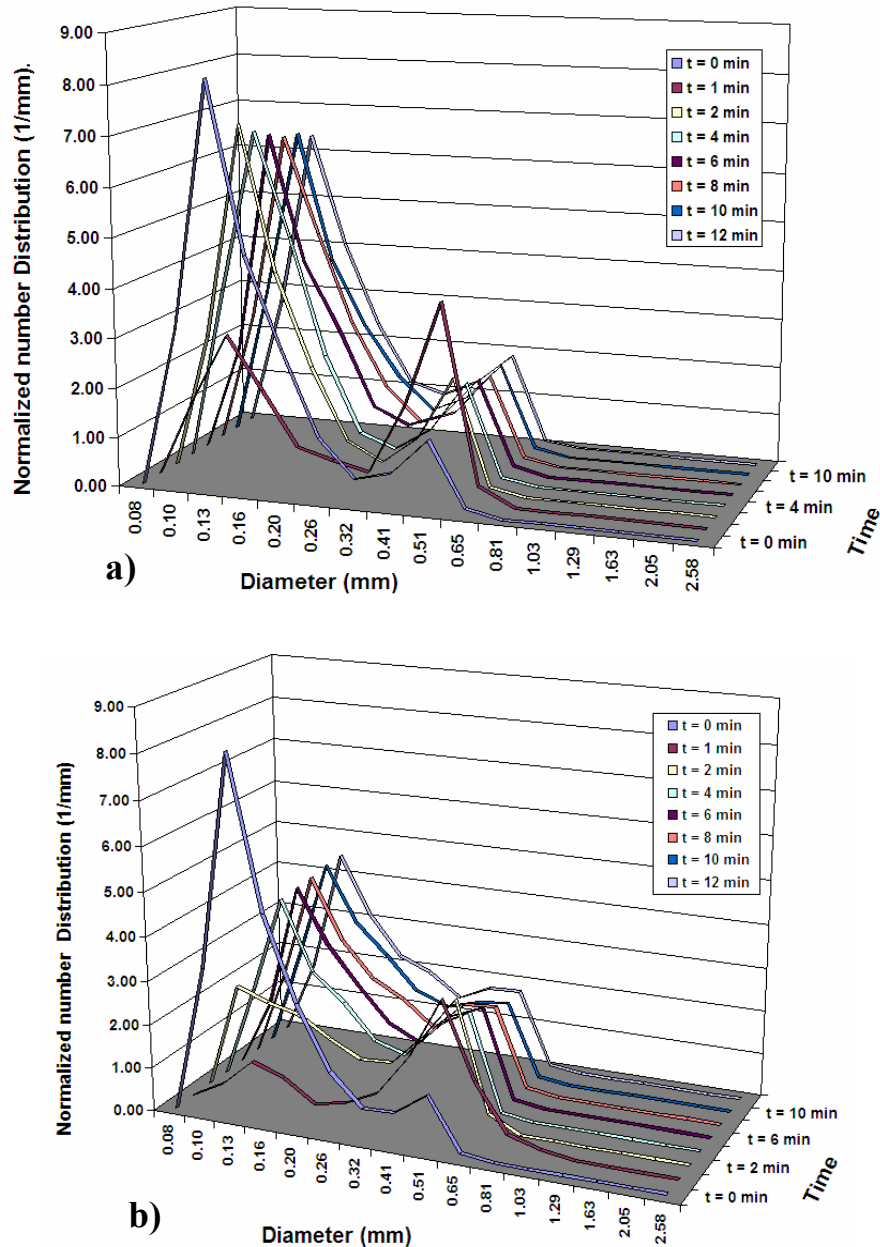


Figure 3.8 Effect of binder content (1 cp viscosity) on wet granulation of coarse size powders (PSD3) with bimodal PSD: a) 9.9% v/w, b) 11.7% v/w and c) 13.6% v/w

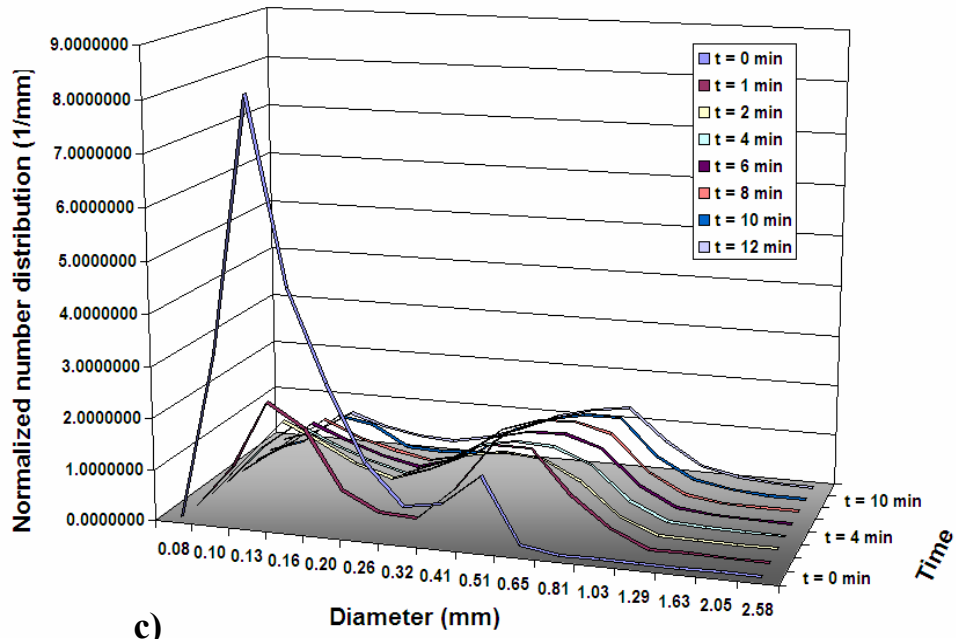


Figure 3.8 (continued)

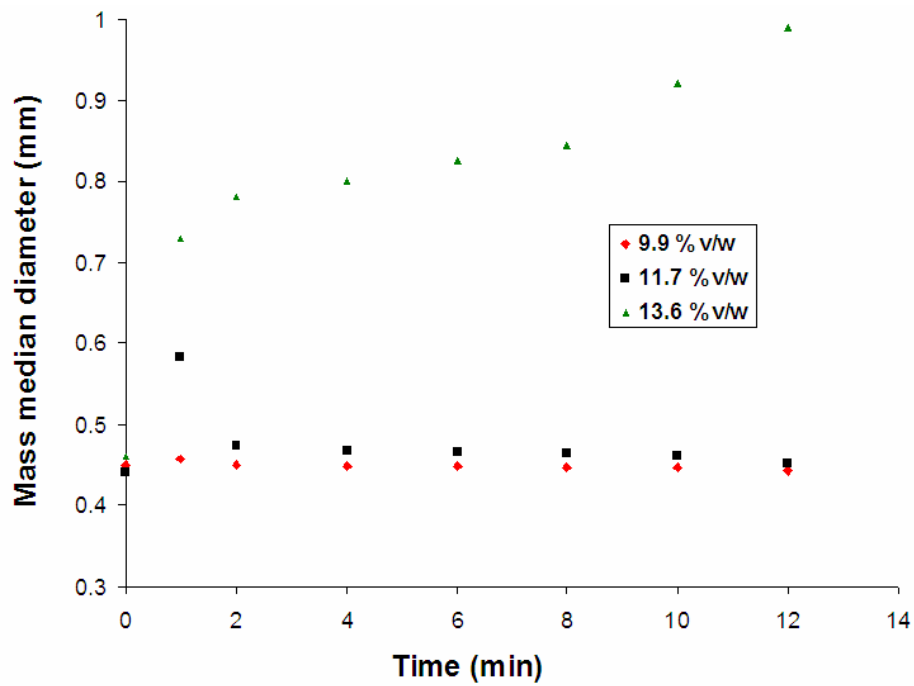


Figure 3.9 Effect of binder content (1 cp viscosity) on wet granulation of coarse size powders (PSD3) with bimodal PSD

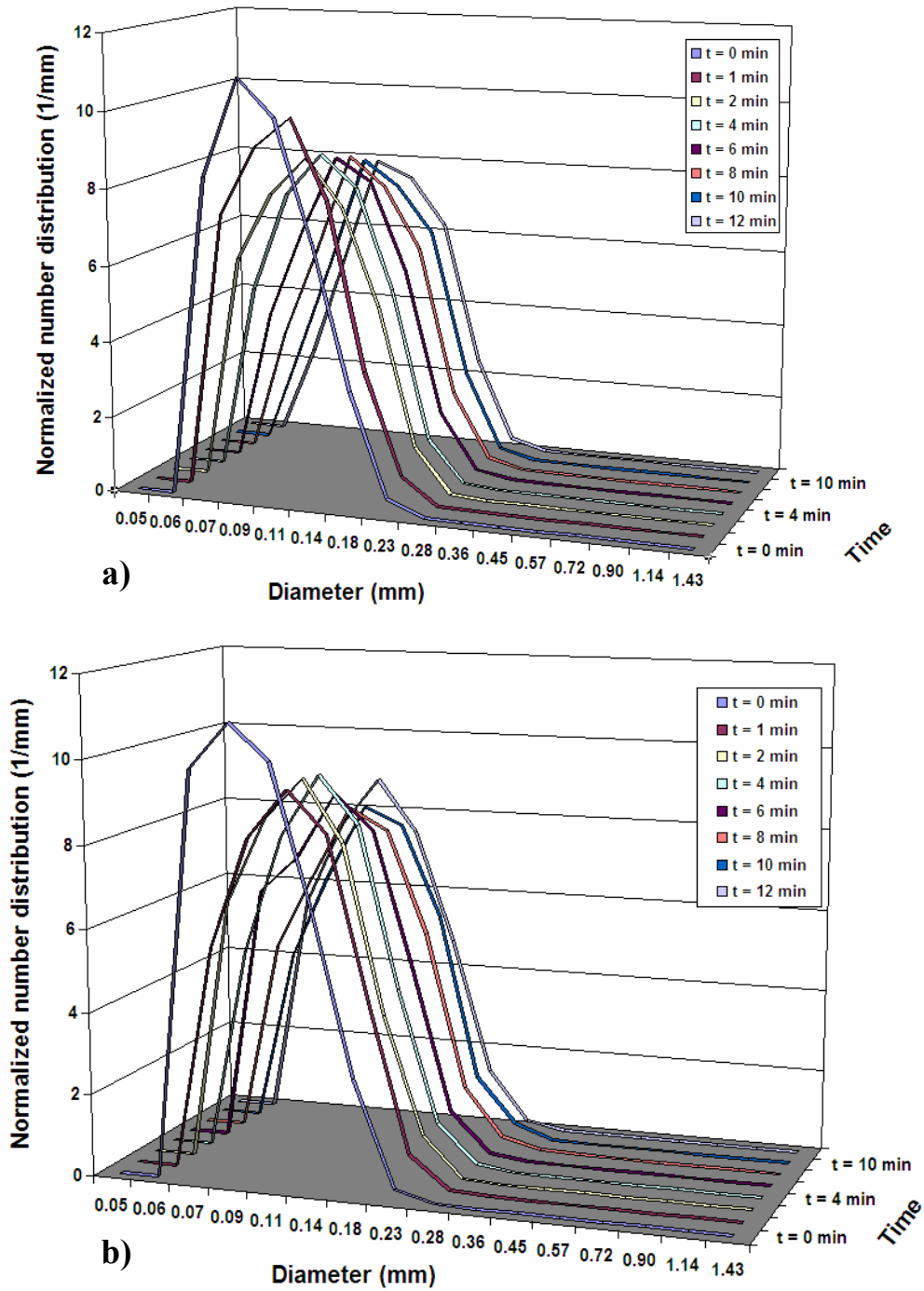


Figure 3.10 Effect of binder content (1 cp viscosity) on wet granulation of fine size powders (PSD1) with unimodal PSD: a) 9.9% v/w, b) 11.7% v/w and c) 13.6% v/w

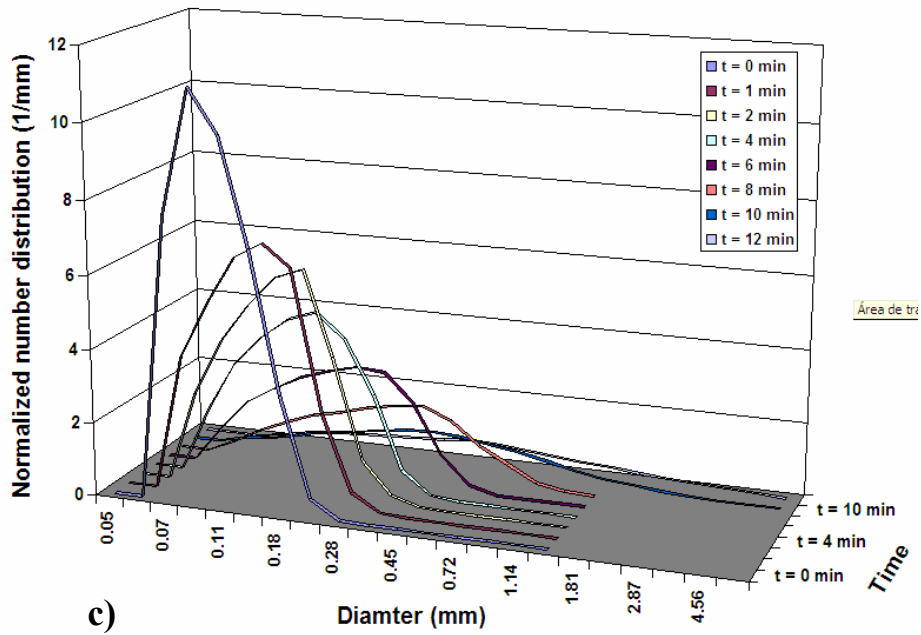


Figure 3.10 (continued)

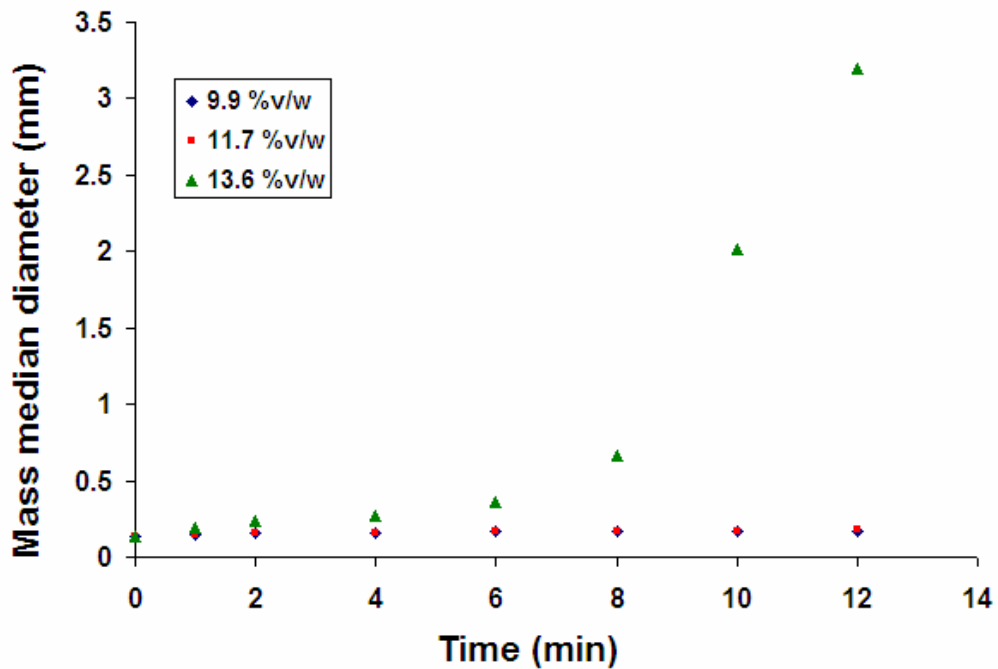


Figure 3.11 Effect of binder content (1 cp viscosity) on wet granulation of fine size powders (PSD1) with unimodal PSD: a) 9.9% v/w, b) 11.7% v/w and c) 13.6% v/w

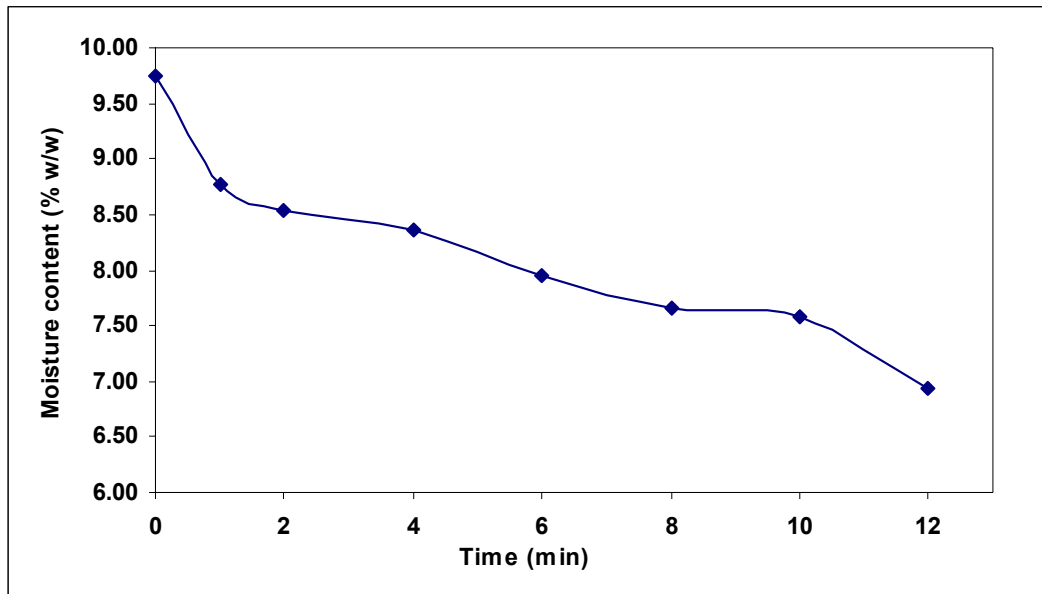


Figure 3.12 Change in binder content (1 cp viscosity) during wet granulation of coarse size powders (PDS3) with bimodal PSD at 9.9% v/w

Figure 3.10 also shows the effect of binder amount at 1 cp viscosity on the growth of particles with unimodal PSD. The agglomeration mechanism was always predominant during wet granulation at three different levels of moisture content. Variations in binder amount can also change the stage number, from one stage at 9.9 and 11.7% v/w of binder, to two stages at 13.6% v/w of binder, as observed in Figure 3.11.

3.4.4 Effect of Binder Viscosity on Granule Growth and the Mechanism of Wet Granulation

Binder viscosity was modified by dissolving different amounts of Povidone in water. Figures 3.13 and 3.14 demonstrate the effect of binder viscosity on the growth kinetics and mechanism of wet granulation of coarse size powders with initial bimodal PSD, at 11.7% v/w of binder. The granulation exhibited a two-stage mechanism: initial fast agglomeration followed by a slow breakage of particles. The growth rate during the first stage increases

with increase in binder viscosity, while the growth rate during the second stage decreases with increase in binder viscosity (Table 3.4 and Figure 3.14).

Table 3.4 Effect of binder viscosity on granule growth rate at 11.7% v/w and coarse size powders (PSD3)

Mass media Diameter (mm)	Viscosity (cp)	Stage	Growth Rate (mm/min)
0.46	1	Second: slow	-0.0009
0.46	2.49	Second: slow	-0.0016
0.46	4.85	Second: slow	-0.0042

The fast granule growth rate is in agreement with results reported by Hoornaert *et al.* [41] when they observed that a viscous binder (water with polyvinylpyrrolidone) produced larger initial granule. Decrease in granule growth rate during the second stage is due to increase of binder viscosity by dissolution of lactose in the binder, which acts as a resistance to the motion of the particle. This favors the binary breakage of particles by high shear of particles. Schaafsma *et al.* [42] suggest that the deviation between the experimental and simulated results in their experiment with a fluid bed granulator was caused by increase in the binder viscosity during wet granulation due to dissolution of lactose in the binder solution.

The large granule size in the first stage, obtained by increase in binder viscosity, is the result of increasing viscous forces, as indicated by Eq. 3.7. It could also be result of the droplet size obtained during binder atomization, achieved by changing the surface tension. However, Holm *et al.* [43] found that granule size in a high shear mixer appears almost independent of atomized binder droplet size.

$$F_{vis} = \frac{3\pi \mu v_0 r_p^2}{4h} \quad 3.7$$

These results are also in agreement with the Stokes number (Eq. 3.2). It has been stated that the coalescence probability increases by increasing binder viscosity covering the

particles. The viscous forces of the binder layer increase as the viscosity increases, as predicted by Eq. 3.7, favoring dissipation of kinetic energy by preventing rebound and allowing the granule to stay in contact long enough for coalescence to occur.

The second stage is characterized by a slow breakage mechanism, due to low binder content (11.7% v/w), which yields rigid granules that break by impact with the blades. Each granule undergoes bimodal breakage to produce many small particles and a few large particles (Figure 3.15a) or many small particles and one large particle (Figure 3.15b). This hypothesis is supported by the decrease noted in large particles and the increase in small and medium size particles, as shown in Figure 3.12. Similar bimodal breakage was also suggested by Hounslow *et al.* [31].

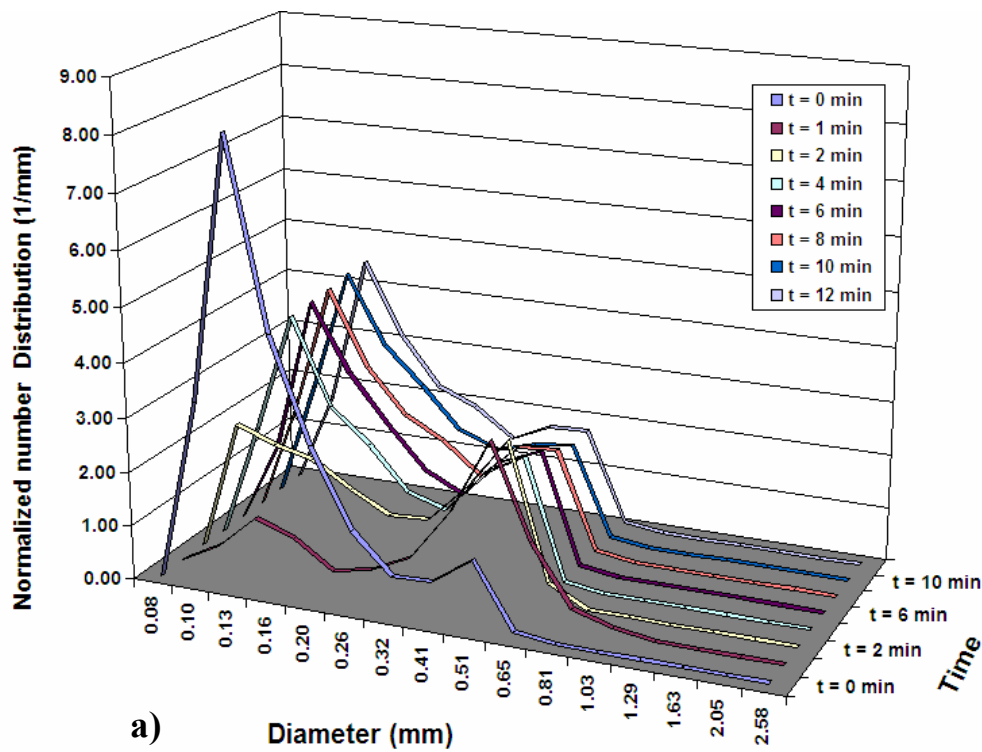


Figure 3.13 Effect of binder viscosity on wet granulation of coarse size powders (PSD3) with initial bimodal PSD at 11.7% v/w

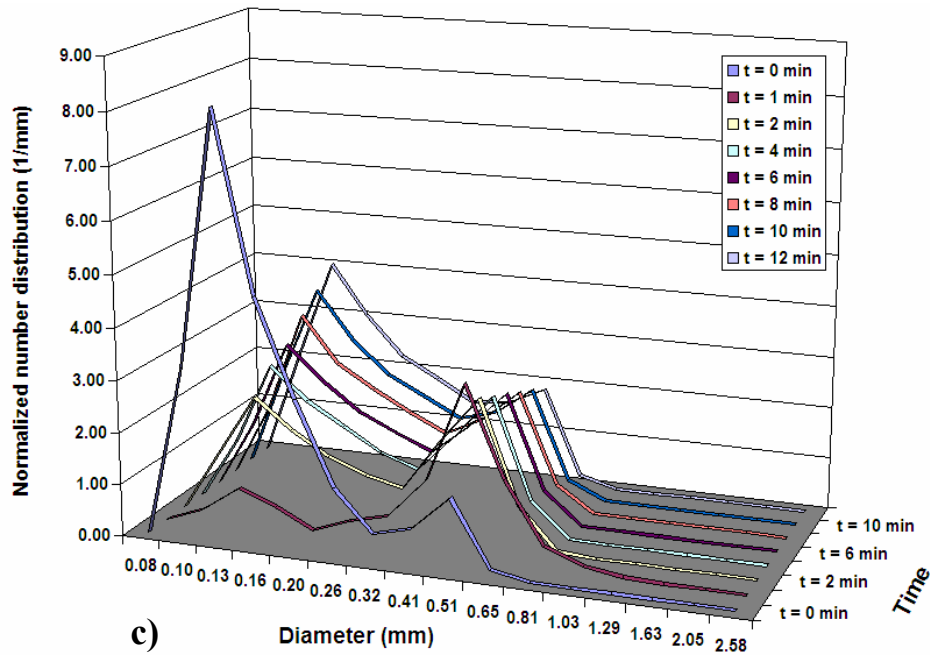
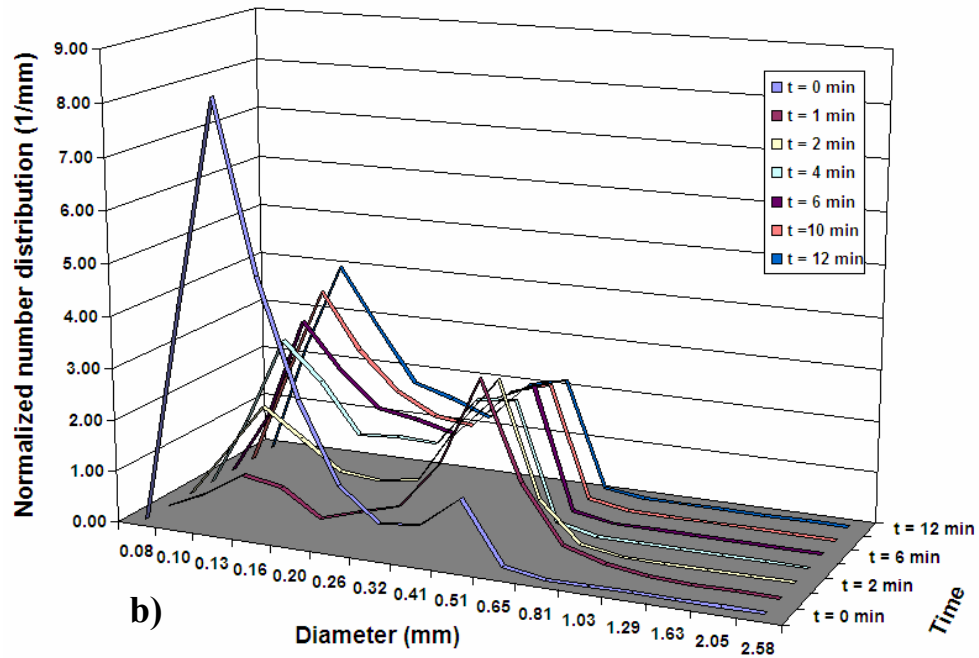


Figure 3.13 (continued)

Figure 3.16 shows the effect of binder viscosity on the growth of particles, in this case, for initial unimodal PSD. The agglomeration mechanism of two stages (medium-fast and

slow growth) was predominant, and the mass median size increased with an increase in binder viscosity during wet granulation. Still, the mechanism of the two stages in wet granulation of powders with unimodal PSD is less pronounced than for powders with bimodal PSD.

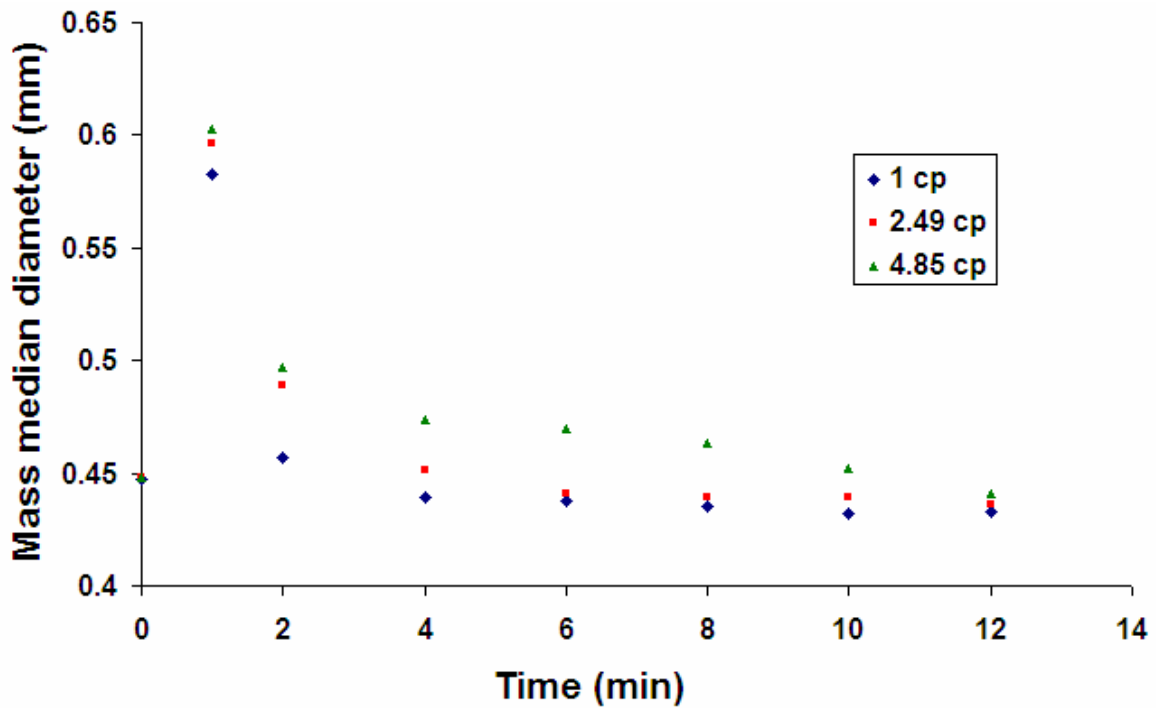


Figure 3.14 Effect of binder viscosity on wet granulation of coarse size powders (PSD3) with initial bimodal PSD at 11.7% v/w

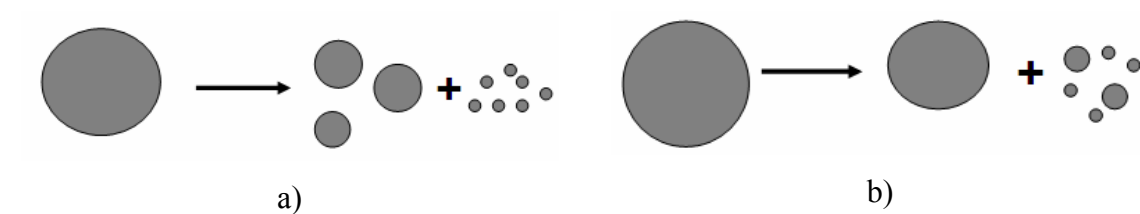


Figure 3.15 Bimodal breakage, a) many small particles and a few large particles, and b) many small particles and one large particle.

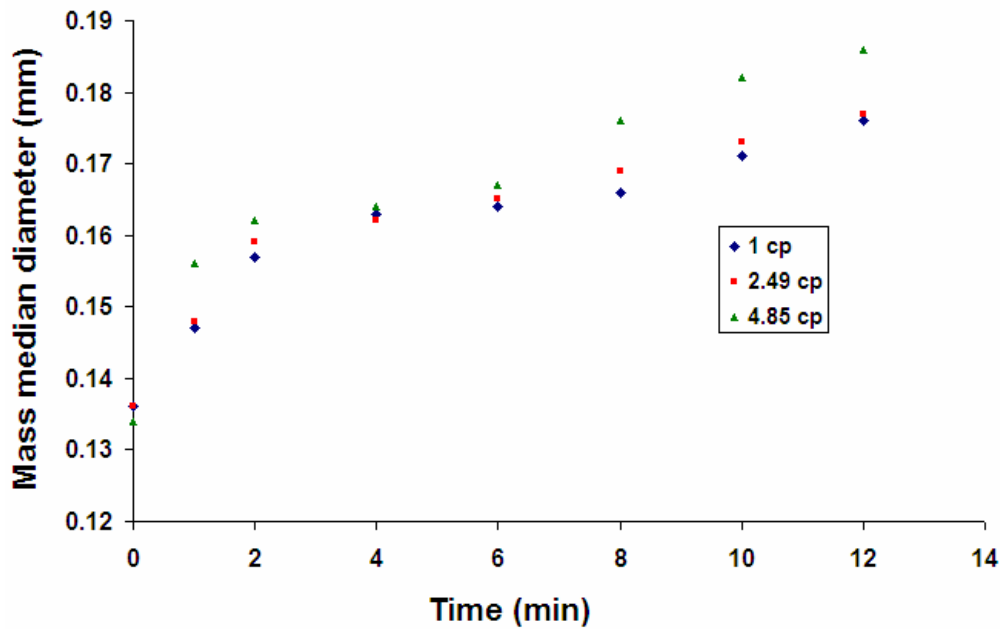


Figure 3.16 Effect of binder viscosity on wet granulation of fine size powders (PSD1) with initial unimodal PSD at 11.7% v/w

3.4.4.1 *Effect of High Binder Viscosity and High Binder Content on the Wet Granulation Process*

The effect of binder viscosity on the enlargement of particles with initial unimodal and bimodal PSD at 13.6% v/w of binder content is very complex and difficult to quantify because granule growth is uncontrollable and also due to low power of the impeller motor to continue the granulation process. Granulation of powder using binder with viscosities of 2.49 and 4.85 cp require an impeller motor of higher power in order to move granules of high cohesivity, which act as resistance to the movement of blades. The granulation process stopped at 8 minutes for binder viscosity of 2.49 cp and at 4 minutes for binder viscosity of 4.85 cp, as shown in Figures 3.17b, 3.17c and 3.18.

The Student's t-test was used to determine whether the mass median diameter measurements of a sample and its replicate give the same or different results. The Student's t-test indicates that the sample and its replicate (Table B.0.1 in Appendix B) are significantly

different at the 95% confidence level for granulation experiments at 13.6% v/w of binder content with 2.49 and 4.85 cp viscosities. In contrast, the Student's t-test indicates that, if experiments with 2.49 and 4.85 cp viscosities at 13.6% v/w of binder content are not included in the statistical analysis, the sample and its replicate are not significantly different. The high precision of the mass median diameter measurements is also confirmed with the analysis of variance (ANOVA) presented in Table B.0.2 (Appendix B) with a standard deviation of 0.01722 mm

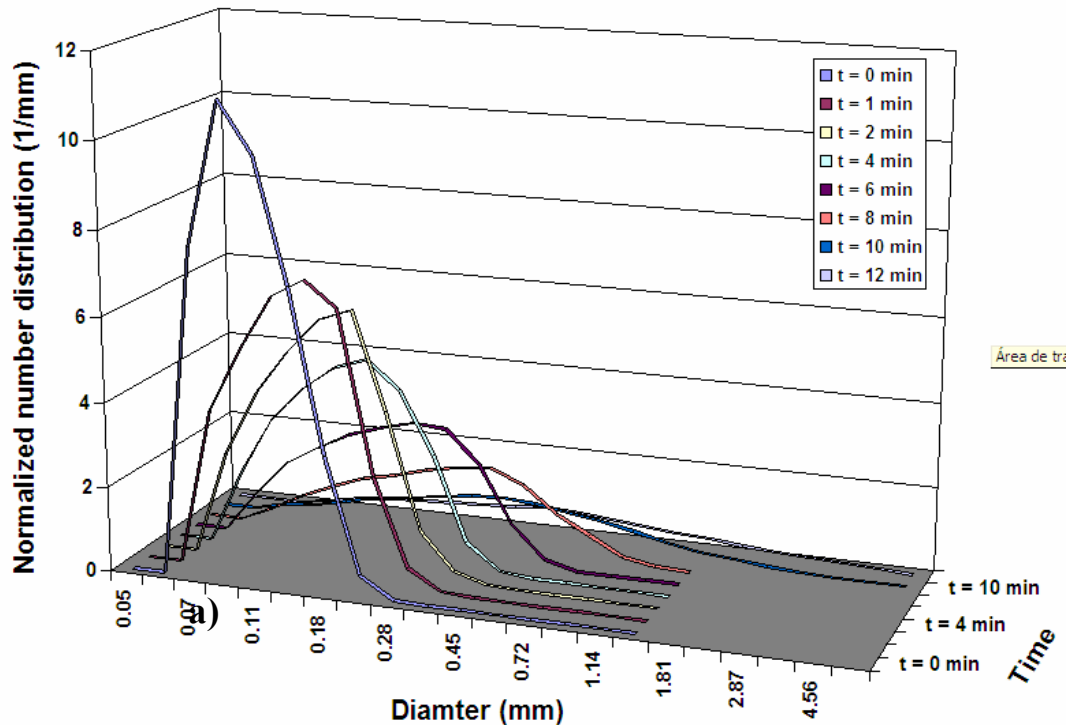


Figure 3.17 Effect of binder viscosity on wet granulation of fine size powders (PSD1) with initial unimodal PSD at 13.6% v/w: a) 1 cp, b) 2.49 cp and c) 4.85 cp.

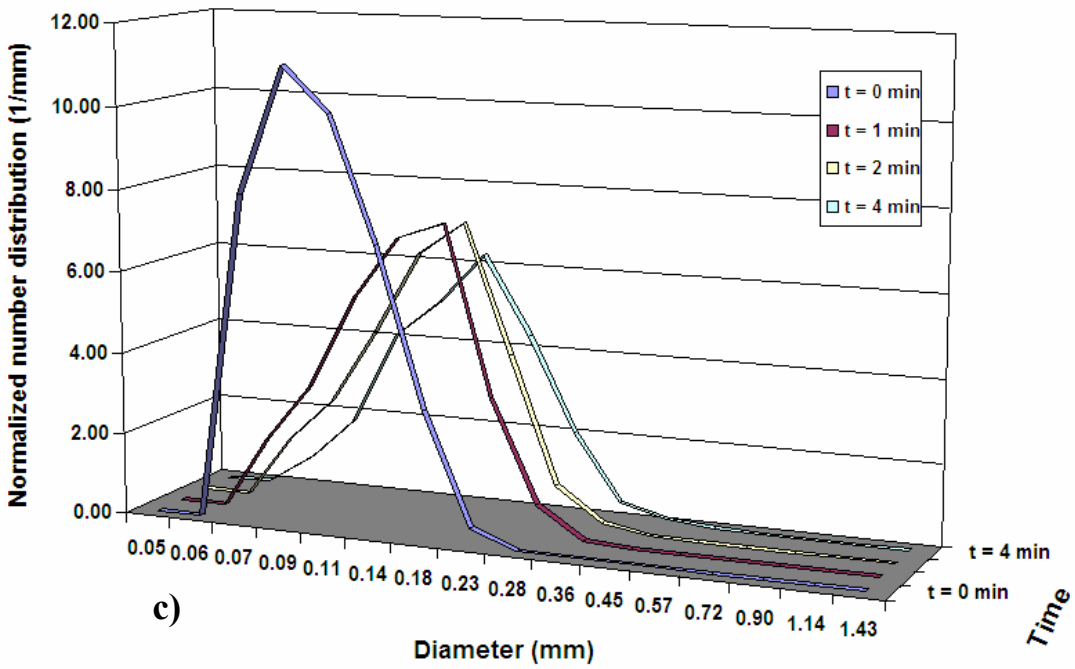
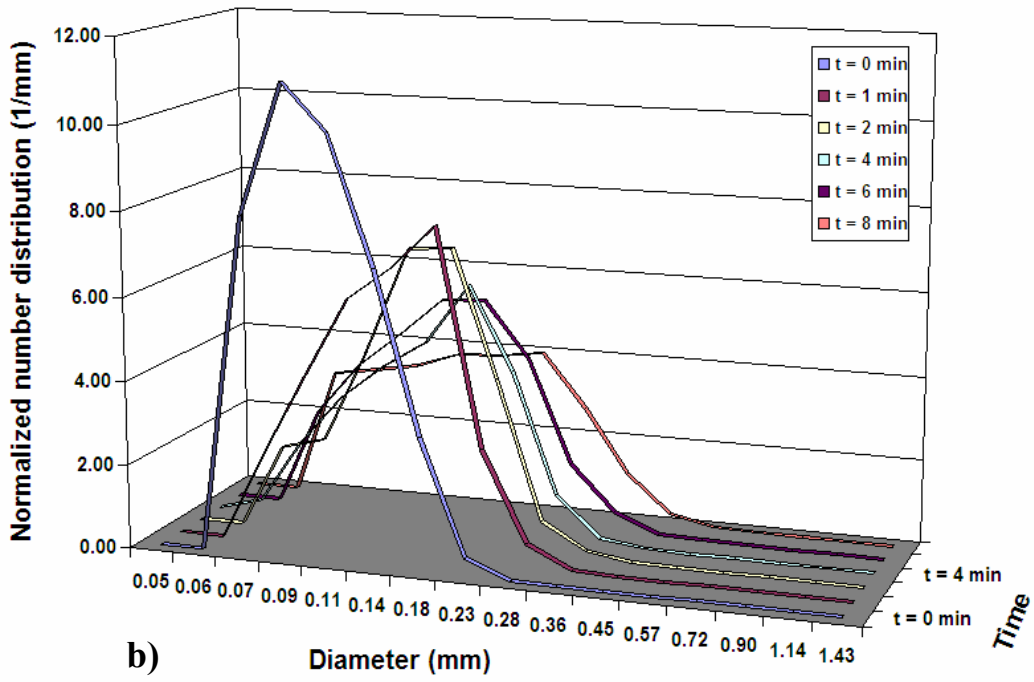


Figure 3.17 (continued)

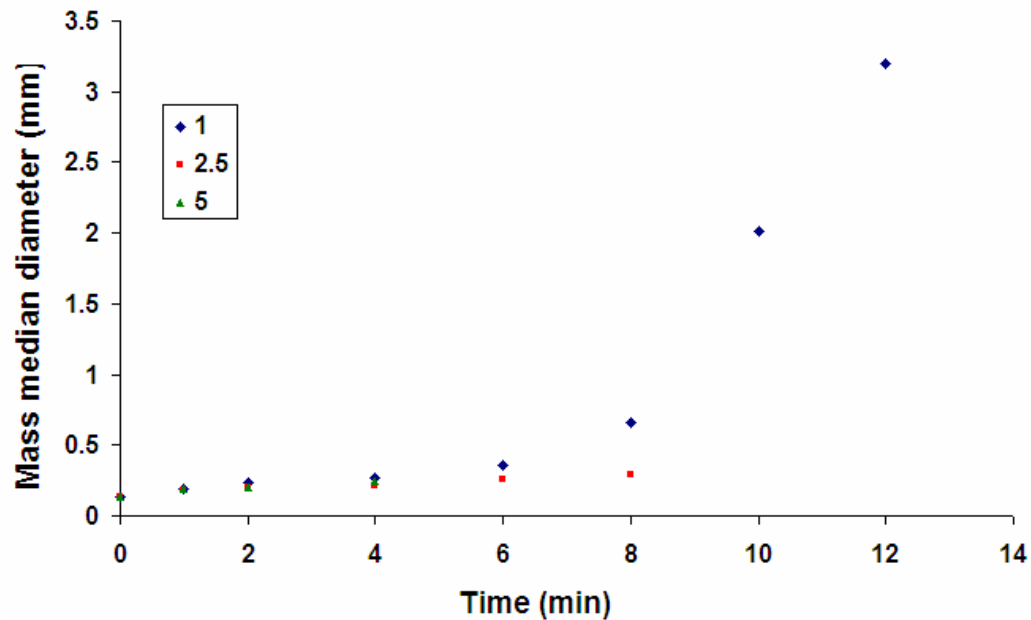


Figure 3.18 Effect of binder viscosity on wet granulation of fine size powders (PSD1) with initial unimodal PSD at 13.6% v/w: a) 1 cp, b) 2.49 cp and c) 4.85 cp.

3.4.5 Description of Experimental Data, using the Agglomeration Kernels Proposed in the Literature

As indicated above, the particle coalescence that occurs during the wet granulation process is favored by the collision between small and large particles, as demonstrated by the higher granule growth rate for powders with bimodal PSD than for powders with unimodal PSD. Table 3.5 shows the three size-dependent kernels published in the literature used to predict our experimental results relative to the stage of slow granule growth. These experimental results were obtained for wet granulation of powders with both unimodal and bimodal PSD. The coalescence kernels were divided into three types: 1) kernels that favor growth rate by collision between small and large particles [32]; 2) kernels that favor growth rate by collision between particles of similar size (Golovin variation); and 3) kernels without preferential effect on growth rate by collision of particles of any size [44].

Table 3.5 also shows the residuals obtained for each kernel by fitting the parameters with experimental data. The parameter estimation was performed using Parsival[®], a commercial software designed to solve a large class of integro-differential equations using the discretization technique. A detailed description is given by Wulkow *et al.* [45]. As anticipated, the Golovin variation and Smoluchoski kernels do not describe the granule agglomeration produced by collision between different-size particles, as observed in Figure 3.19, which reveals results only at 12 minutes. The Hounslow's kernel describes the experimental data obtained from wet granulation of fine and medium size powders, but it does not describe the first peak in the curve for wet granulation of coarse size powders at the endpoint of the experiment.

Table 3.5 Goodness of fit for kernels, relative to the experimental data

<i>Kernel structure</i>	<i>Reference</i>	<i>Average Residuals</i>		
		<i>Unimodal PSD1</i>	<i>Bimodal PSD2</i>	<i>Bimodal PSD3</i>
$(l + \varepsilon)^3$	Smoluchoski [24]	9.6083×10^{-2}	6.0243×10^{-1}	4.0120×10^{-1}
$(l \times \varepsilon)$	Golovin variation	8.7336×10^{-2}	6.0247×10^{-1}	4.0140×10^{-1}
$(l + \varepsilon)^2 \times \sqrt{\left(\frac{1}{l^3} + \frac{1}{\varepsilon^3}\right)}$	Equipartition of kinetic energy. Boerefijn and Hounslow [32]	8.7284×10^{-2}	1.6876×10^{-1}	1.7822×10^{-1}

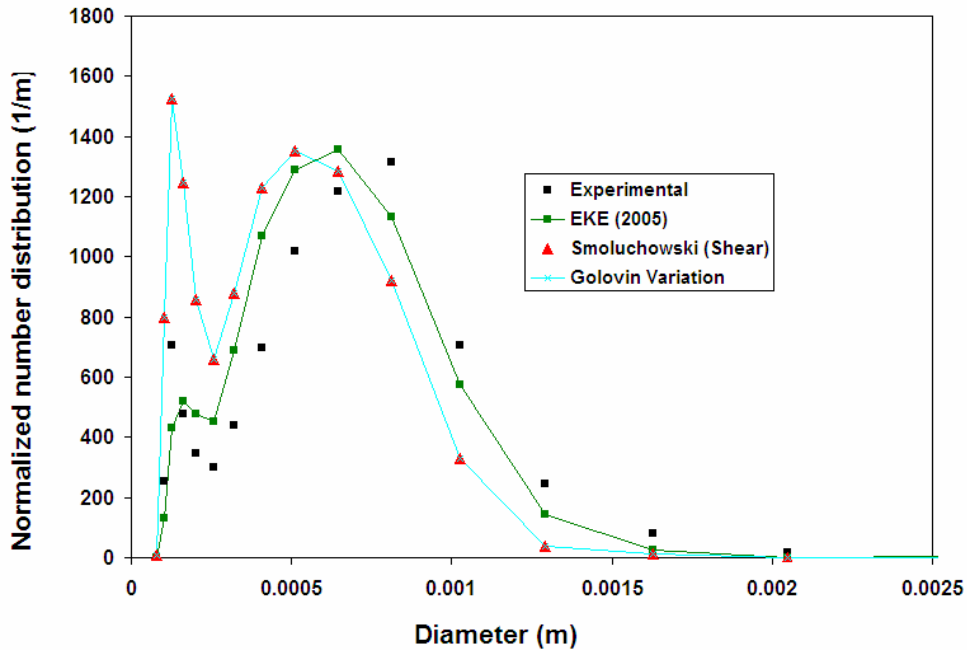


Figure 3.19 Comparison of simulations of coalescence kernels published in the literature versus the experimental data (bimodal PSD3)

3.5 Conclusions

Initial PSD shape, whether unimodal or bimodal, has a strong effect upon granule growth rate and the mechanism by which wet granulation occurs. A sequential mechanism consisting of two stages was observed during the wet granulation of powders with bimodal PSD, for three binder contents. The first stage of rapid granule growth is controlled by the binder amount and by the high probability of coalescence resulting because of collision of small and large particles. The second stage exhibits slow agglomeration when binder content is 13.6% v/w, and slow breakage when binder content is 9.9 or 11.7% v/w.

Wet granulation of pharmaceutical powders with initial unimodal PSD, at 9.9 and 11.7% v/w binder content, exhibited slow granule growth rate in two stages, stages which are less pronounced than the two stages for powders with bimodal PSD. In contrast, wet granulation of pharmaceutical powders with initial unimodal PSD at 13.6% v/w binder content exhibited two pronounced stages, due to the enlargement of particles that occurred during the first

stage (the first six minutes) of wet granulation, which transforms the distribution shape from a mono-dispersed, unimodal PSD to a poly-dispersed, unimodal PSD. A volume ratio between small and large particles of approximately 150 was necessary to obtain fast granule growth.

In general, the binder content, PSD shape, and interaction between particle size and binder content were factors with a strong effect upon granule growth rate and the mechanism of wet granulation; whereas binder viscosity and initial particle size affected the granule growth rate moderately. The variation in the three factors is explained by the viscous Stokes' (St_v) number, developed by Ennis *et al.* [25], wherein the probability of successful coalescence between particles is increased by smaller particle size, higher binder viscosity, and higher binder content.

Granule bimodal breakage is caused by the impact of the largest granules with the mixer blades, thereby producing many small particles and a few large particles; or many small particles and one large particle.

The experimental results were best predicted by a population balance equation using a coalescence kernel that favors growth rate by collision between small and large particles.

4 AGGLOMERATION MODELING OF SMALL AND LARGE PARTICLES BY A DIFFUSION THEORY APPROACH

ABSTRACT

The interaction between the particle and binder layer during the wet granulation process is an important factor in the agglomeration of particles. This interaction has been modeled by a force balance acting on the particle where binder's viscous force increases the strength of liquid bridge and facilitates the particle agglomeration. Currently, the binder viscosity, size particle and the ratio between particle sizes (monodisperse and polydisperse) are not considered to develop the kernel coalescence of population balance equation (PBE) which makes difficult the modeling of growth kinetics. In this work, an agglomeration kernel based on Brownian movement of small particles in the binder layer and binder's viscous forces was used to model analytically the wet granulation process of pharmaceutical powders in a laboratory-scale high shear mixer. Considerations no-stationary and pseudo-stationary were suitable to describe growth kinetics of the two stages (fast and slow) observed in wet granulation process of pharmaceutical powders. The model predicts the change of particle size distribution (PSD) during wet granulation by including the initial material properties such as binder viscosity and powder particle size. Also, the binder amount predominant during the fast granule growth is considered indirectly in the variable of binder layer. Simulation results using the theoretical kernel were in good agreement with experimental data.

4.1 Introduction

Wet granulation is the process of particle size growth by means of addition of liquid or solid binder [32]. It is widely used in many chemical industries including pharmaceutical, food, detergents and agricultural. The change in particle size as a function of time during the

wet granulation process can be modeled by the population balance equation (PBE) as established by Randolph and Larson [4]:

$$\frac{\partial n}{\partial t} + \frac{\partial(Gn)}{\partial l} + \nabla \cdot (vn) - B + D = \frac{1}{V} (\sum Q_{in} \times n_{in} - \sum Q \times n) \quad 4.1$$

where n is the number density function, t is the time, G is the growth rate, l is a length of particle, v is the particle velocity, B and D are the birth and death rate respectively, V is the mixer volume, Q_{in} and Q are the inlet and outlet flow rates, respectively. The PBE reduces to Eq. 4.2 for the case of agglomeration alone in a well-mixed batch granulator with the birth and death terms given by Hulburt and Katz [46]:

$$\frac{\partial n(l)}{\partial t} = \frac{1}{2} \int_0^l \beta(l-\varepsilon, \varepsilon) \times n(l-\varepsilon) \times n(\varepsilon) \times d\varepsilon - n(l) \int_0^\infty \beta(l, \varepsilon) \times n(\varepsilon) \times d\varepsilon \quad 4.2$$

where $\beta(l, \varepsilon)$ is the coalescence kernel for agglomeration between particles of size l and ε . The $\frac{1}{2}$ in the first term avoids the duplication in the number of collisions. Satry and Fuerstenau [47] decomposed the coalescence kernel into two terms as:

$$\beta(l, \varepsilon, t) = \beta_0(t) \beta'(l, \varepsilon) \quad 4.3$$

where $\beta_0(t)$ is the aggregation rate constant, which is a function of factors such as binder viscosity and amount, and impeller velocity, and $\beta'(l, \varepsilon)$ expresses the effect of size on the rate of aggregation between particles of size l and ε .

The current challenge in modeling growth kinetics has to do more with the quantification and physical interpretation of coalescence kernels of wet granulation processes. Table 4.1 shows a list of size-dependent kernels obtained empirically, semi-empirically or from semi-theoretical concepts. The parameters of the size-dependent kernel and the aggregation rate constant ($\beta_0(t)$) value are both calculated by fitting of experimental data. Due to the lack of fundamental understanding to model particle agglomeration, wet granulation in a high shear mixer is controlled by monitoring the impeller torque [48, 49].

The main objective of this work is to develop an agglomeration kernel of wet granulation applying the random motion theory and viscous force of liquid bridge between

two particles. In addition, the prediction of the developed kernel will be compared to experimental data.

Table 4.1 Size-dependent kernels obtained empirically, semi-empirically or from semi-theoretical concepts

Kernel structure	Reference
1	Size independent
$\beta_0(t)(l + \varepsilon)^3$	Smoluchowski [44]
$\beta_0(t)(l + \varepsilon)$	Golovin [50]
$\beta_0(t)(l \times \varepsilon)$	Golovin variation
$\beta_0(t) \frac{(l + \varepsilon)^a}{(l \times \varepsilon)^b}$	Kapur [51]*
$\begin{cases} \beta_0(t) & t < t_1 \\ \beta_0(t)(l + \varepsilon) & t > t_1 \end{cases}$	Adetayo et al. [28]*
$\beta_0(t)(l^{1/3} + \varepsilon^{1/3}) \times \sqrt{\left(\frac{1}{l} + \frac{1}{\varepsilon}\right)}$	EKE: Kinetic theory of gases-equipartition of kinetic energy. Hounslow et al. [31]
$\beta_0(t)(l + \varepsilon)^2 \times \sqrt{\left(\frac{1}{l^3} + \frac{1}{\varepsilon^3}\right)}$	Equipartition of kinetic energy. Boerefijn and Hounslow [32]

*a, b are parameters, and t_1 was calculated experimentally

4.2 Development of Agglomeration Kernel: Theoretical Analysis

4.2.1 Agglomeration of Particles

The process of mono-dispersed aerosol coagulation (Figure 4.1a) as established by Smoluchowski [44] is equivalent to the process of agglomeration between small and large

particles as shown in Figure 4.1b. The agglomeration of large and small particles in the presence of binder on the surface of particles is considered by Tardos et al. [30] and Mills et al. [27] in their proposed layering mechanism. Hounslow et al. [31], and Boerefijn and Hounslow [32] also considered the agglomeration of large and small particles through their size-dependent agglomeration kernel (see Table 1). The preferential agglomeration of small and large particles (volume ratio = 150) was also observed in the wet granulation of pharmaceutical powders with initial bimodal PSD (see previous chapter). Similar behavior was observed for powders with poly-dispersed unimodal PSD, with a volume ratio of small to large particles of approximately 150, after certain time of granulation (see previous chapter).

Independently of the high particle transfer by the convection mechanism in a high particle concentration volume, the agglomeration process is governed by particle diffusion through the binder layer. Furthermore, let us assume a particle population of radius r_{p2} diffusing to a stationary particle of radius r_{p1} through the binder layer on the particle surface. According to the preferential agglomeration of small and large particles, the diffusion of small particles (radius r_{p2}) through the binder layer follows the Brownian movement [52, 53, 54], which is the physical phenomenon that minute particles, immersed in a fluid, move about randomly.

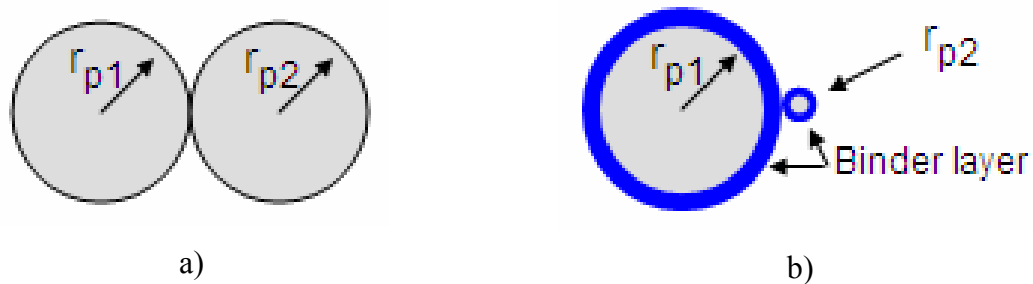


Figure 4.1 Schematic of aggregation of (a) equal-size particles and (b) different-size particles

The system shown in Figure 4.1-b can be represented mathematically by the following diffusion equation:

$$\frac{\partial N_2(r,t)}{\partial t} = D_{12} \left(\frac{\partial^2 N_2(r,t)}{\partial r^2} + \frac{2}{r} \frac{\partial N_2(r,t)}{\partial r} \right) \quad 4.6$$

where N is the concentration number of particles, r is the distance from the center of the stationary particle to the center of the diffusing particles, D_{12} is the Brownian diffusion constant of particles through the binder layer. The initial and boundary conditions for the problem are:

$$N_2(r,0) = N_{2,0} \quad 4.7$$

$$N_2(\infty, t) = N_{2,0} \quad 4.8$$

$$N_2(r_{p1} + r_{p2}, t) = 0 \quad 4.9$$

The solution of Eq. 4.6 using the initial and boundary conditions is:

$$N_2(r,t) = N_{2,0} \left(1 - \frac{r_{p1} + r_{p2}}{r} \operatorname{erf} \left(\frac{r - (r_{p1} + r_{p2})}{2\sqrt{D_{1,2}t}} \right) \right) \quad 4.10$$

The collision rate of particles with the stationary particle of surface area $A = 4\pi(r_{p1} + r_{p2})^2$ is given by the total flux, I , to surface of the reference particle:

$$r_{col} = I = A \times J \quad 4.11$$

where the flux, J , is:

$$J = D_{12} \left(\frac{\partial N}{\partial r} \right)_{r=r_{p1}+r_{p2}} \quad 4.12$$

Replacing the surface area and flux in Eq. 4.11, one obtains

$$r_{col} = 4\pi(r_{p1} + r_{p2})^2 D_{12} \left(\frac{\partial N}{\partial r} \right)_{r=r_{p1}+r_{p2}} \quad 4.13$$

The collision rate of particles of radius r_{p2} that collide with a single particle of radius r_{p1} is given by:

$$r_{col-1r_{p1} \bullet r_{p2}} = 4\pi(r_{p1} + r_{p2}) D_{12} N_{2,0} \quad 4.14$$

The total collision rate per volume between particles of radius r_{p1} with concentration number $N_{1,0}$ and particles of radius r_{p2} is given by,

$$r_{col-r_{p1},r_{p2}} = 4\pi(r_{p1} + r_{p2})D_{12} N_{2,0} N_{1,0} \quad 4.15$$

Rewriting Eq. 4.15 as:

$$r = \beta(v_1, v_2)N_1N_2 \quad 4.16$$

one obtains

$$\beta(r_{p1}, r_{p2}) = 4\pi(r_{p1} + r_{p2})(D_1 + D_2) \quad 4.17$$

Einstein [52, 53] related the diffusion constant (D_i) to the average square displacement given by Eq. 4.18. The mean square displacement is a measure of the average distance a particle travels suspended in air or liquid. In this case as established above, the particles is diffusing through the binder layer.

$$D_i = \frac{\langle x^2 \rangle}{2t} \quad 4.18$$

The average square displacement can be obtained by analyzing the effect of viscous forces on the motion of particles through viscous liquid layer as presented in the sections below.

4.2.2 *Agglomeration Mechanism based on Brownian Movement and Viscous Forces*

Two-stage granule growth has been observed in wet granulation of wide PSD by Ennis et al. [25], Adetayo et al. [28] and the granulation experiments presented in previous chapter. The first stage of wet granulation is a non-inertial regime of fast granule random coalescence and it is controlled by binder amount. The granule growth occurring by random coalescence has been reported by Ennis et al. [25], Kapur and Fuerstenau [55]. The second stage is characterized by slow agglomeration and described by a pseudo-stationary coalescence [25].

4.2.2.1 Modeling the First Stage of Fast Granule Growth of Wet Granulation

The interaction of particles with the binder layer during the first stage of wet granulation process can be analyzed by a force balance acting on the particle as established by Ennis et al. [25, 26] where a viscous force favors particle motion and also considering the stochastic Brownian force X as used by Langevin [56], which is randomly positive and negative, since it represents the random force exerted by other particles in the wet granulation process. This random force maintains the motion of particle through the binder layer and this motion can be modeled by Eq. 4.19:

$$m_p \frac{d^2 x}{dt^2} = \frac{3\pi \times \mu \times r_p^2}{2x} \frac{dx}{dt} + X \quad 4.19$$

where μ is the binder viscosity, m_p is the particle mass, r_p is the particle radius, and $2x$ is the separation distance between colliding granules. The initial conditions are:

$$x(0) = h_0 \quad 4.20$$

$$\frac{dx}{dt}(0) = v_0 \quad 4.21$$

where h_0 is the thickness of the liquid layer on the surface of the particle and v_0 is the relative velocity between the two particles. Multiplying Eq. 4.19 by x , one obtains:

$$m_p(x) \frac{d^2 x}{dt^2} = \frac{3\pi \times \mu \times r_p^2}{2} \frac{dx}{dt} + Xx \quad 4.22$$

Considering a large number of particles, then the average of the term Xx is zero by irregularity of direction of forces X as established by Langevin [56, 57]. Hence, the equation may be rewritten as:

$$\frac{d^2 x^2}{dt^2} = 2 \left(\frac{dx}{dt} \right)^2 + \frac{6\pi \times \mu \times r_p^2}{2m_p} \left(\frac{dx}{dt} \right) \quad 4.23$$

Assuming validity of the equipartition of kinetic energy principle during wet granulation as proposed by Boerefijn and Hounslow [32], where the collision velocity, v , is inversely proportional to the particle mass, m , one obtains

$$m_p v^2 = C \Rightarrow v^2 = \frac{C}{m_p} \Rightarrow v = \sqrt{\frac{C}{m_p}} \quad 4.24$$

where C is a constant in energy unit.

Replacing Eq. 4.24 into 9.23 and $m_p = 4/3 \pi r_p^3$, one obtains

$$\frac{d^2 x^2}{dt^2} = \frac{6C}{4\pi \rho r_p^3} + \frac{9\mu}{8\rho r_p} \sqrt{\frac{3C}{4\pi \rho r_p^3}} \quad 4.25$$

The analytical solution using the initial conditions (Eqs. 4.20 and 4.21) is:

$$x^2 = \left[\left(\frac{3c}{4\pi \rho r_p^3} \right) + \frac{9\mu}{16\rho r_p} \sqrt{\frac{3c}{4\pi \rho r_p^3}} \right] t^2 + 2h_0 v_0 t + h_0^2 \quad 4.26$$

Replacing the mean square displacement (x^2) of Eq. 4.18, one obtains the diffusion coefficient for each particle.

$$D_i = \left[\left(\frac{3c}{8\pi \rho r_{pi}^3} \right) + \frac{9\mu}{32\rho r_{pi}} \sqrt{\frac{3c}{4\pi \rho r_{pi}^3}} \right] t + h_0 v_0 + \frac{h_0^2}{2t} \quad 4.27$$

4.2.2.2 Modeling the Stage of Slow Granule Growth of Wet Granulation

The second stage is characterized by slow agglomeration and described by a pseudo-stationary coalescence as observed by Ennis et al. [25], Adetayo et al. [28], Schaafsma et al. [42]. The interaction of particles with the binder layer during the second stage of wet granulation process can be modeled by a force balance acting on the particle. In this case, the viscous liquid force acts as a resistance to the motion of particle [56, 57]. The motion of particles through the binder layer can be modeled by Eq. 4.28:

$$m_p \frac{d^2 x}{dt^2} = -6\pi \mu r_p \frac{dx}{dt} + X \quad 4.28$$

Multiplying Eq. 4.28 by x , Eq. 4.29 is obtained

$$\frac{m_p}{2} \frac{d^2 x^2}{dt^2} - m_p v^2 = -3\pi \mu r_p \frac{dx^2}{dt} + Xx \quad 4.29$$

Applying the equipartition of kinetic energy (Eq. 4.24), the average over a large number of particles of $Xx=0$ and with the following change in variable $z = dx^2/dt$, the equation becomes

$$\frac{dz}{dt} + \frac{6\pi \mu r_p}{m_p} z = \frac{2C}{m_p} \quad 4.30$$

The general solution using the integrating factor technique is:

$$z = \frac{C}{3\pi \mu r_p} + C_1 e^{-\frac{6\pi \mu r_p t}{m_p}} \quad 4.31$$

For $t \gg 6\pi \mu r_p / m_p$, the particle velocity enter to a pseudo-stationary state. In this case the exponential is dropped and integrating for time again.

$$x^2 = \frac{C}{3\pi \mu r_p} t \quad 4.32$$

Replacing the mean square displacement (x^2) of Eq. 4.18, the diffusion coefficient for each particle is

$$D_i = \frac{C}{6\pi \mu r_{pi}} \quad 4.33$$

Replacing the diffusion coefficient (Eq. 4.33) into Eq. 4.17, the coalescence kernel becomes

$$\beta(r_{p1}, r_{p2}) = \frac{C (r_{p1} + r_{p2})^2}{\mu (r_{p1} \times r_{p2})} \quad 4.34$$

4.3 Solution of the Population Balance Equation

Since the PBE is an integro-differential equation difficult to solve analytically for real cases, a numerical solution was implemented using PARSIVAL, a commercial software to solve a large class of integro-differential equations using a discretization technique. A detailed description is given by Wulkow et al. [45]. The algorithm uses a finite-element type Galerkin h–p-method and applies an adaptive Rothe method for a time discretization. Then in

each time step a linear time independent partial differential equation system is solved using the Gaussian quadrature method. The next time-step is calculated based in the accuracy that is demanded for the overall time dependent solution.

4.4 Results and Discussion

Agglomeration kernel simulation results were compared to the granulation experiments presented in the previous chapter where the agglomeration mechanism occurs. Pharmaceutical powders with unimodal and bimodal PSD were used in the experiments of wet granulations that included lactose anhydrous, and lactose monohydrate. Figure 4.2 depicts three particle size distributions used in wet granulation, designated as PSD1 (fine size powders), PSD2 (medium size powders) and PSD3 (coarse size powders). The binder viscosity and amount were also changed in three levels as shown by the factorial experimental design [17] in Table 4.2.

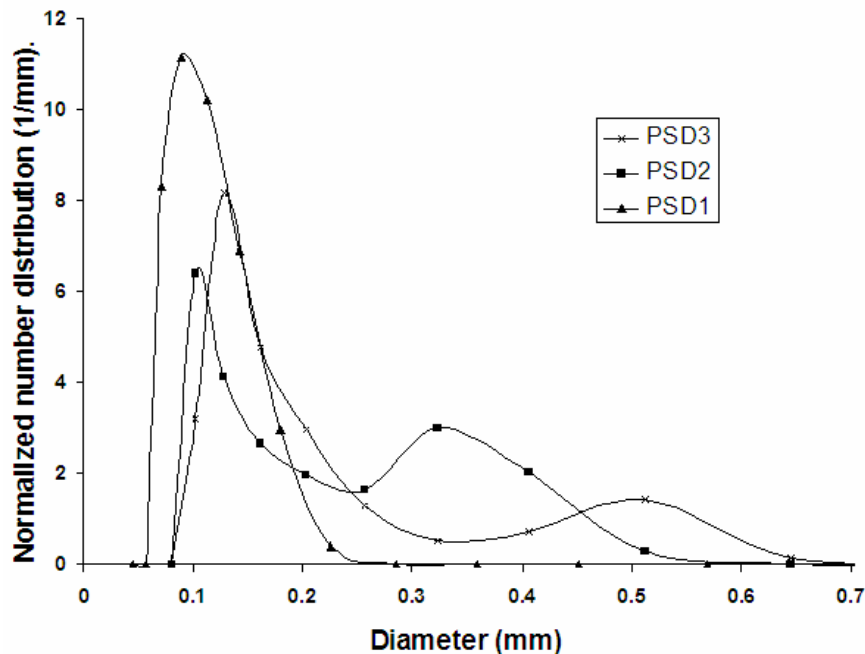


Figure 4.2 Initial particle size distributions for wet granulation

Table 4.2 Experimental Design

Factors	Particle size (mm). Figure 2.1			Binder viscosity (cp)			Amount of binder (% V _{Liquid} /W _{Solid})		
	PSD1	PSD2	PSD3	1	2.49	4.85	9.9	11.7	13.6
Levels									

4.4.1 Comparison of model simulation to experimental data

4.4.1.1 First Stage of Wet Granulation

A complex coalescence kernel for the first fast stage is obtained by replacing Eq. 4.27 into Eq. 4.17. The kernel structure cannot be separated into two terms as suggested by Satry and Fuerstenau [47] but it is a function of liquid viscosity, particle density, liquid amount, particle size and time as suggested also by them. Hounslow et al. [31] found independently by numerical technique a minimal dependence with time of this size-independent kernel ($\beta_0(t)$). As can be seen, the coalescence kernel obtained for the first stage of wet granulation has two parameters (C and h_0). The parameter C has energy unit and is related to the force that maintain the motion of particles, and h_0 is the thickness of a binder layer, which change accordingly to binder amount. Since h_0 would be very difficult to measure experimentally, it is typically estimated numerically.

The coalescence kernel predicts the trend of fast growth, which is controlled by binder amount added during the first 30 seconds and high probability of collision between small and large particles. The C , v_0 , and h_0 values for PSD simulation were obtained by trial and error since the amount of data collected during the first stage did not allow for least square estimation. It would be necessary to obtain more samples during the first two minutes of wet granulation to calculate more accurate parameters by fitting the experimental data. The inline measurements of PSD or to take samples automatically without stopping the granulator are recommended to reduce perturbations in the granulation process.

4.4.1.2 Second Stage of Wet Granulation

The coalescence kernel of wet granulation of powders with bimodal PSD for second stage of slow growth rate is similar to the kernel obtained by Smoluchowski [44], but in this

case, the particle transfer mechanism by diffusion through binder layer was considered. The kernel can be separated in two terms as defined by Satry and Fuerstenau [47], β_0 is the aggregation rate constant, which is a function of binder viscosity and the C parameter as defined above, and $\beta'(r_{p1}, r_{p2})$ expresses the effect of size on the rate of aggregation between particles of size r_{p1} and r_{p2} .

The C value of $3.6915 \times 10^{-13} \text{ m}^2 \text{ Kg min}^{-2}$ was extracted by fitting the coalescence kernel (Eq. 4.33) to PSD experimental data using the integral technique of the Parsival software [45]. Table 4.3 shows two kernel structures proposed in literature and the one developed here (random kernel, Eq. 4.34). Table 4.3 compares quantitatively the goodness of the kernels on fitting parameters to experimental data. Figure 4.3 depicts qualitatively the prediction of some kernels published in literature to experimental data obtained from wet granulation of coarse size powders (PSD3) at 13.6 %v/w of binder and 1 cp. The random kernel gives the best description of experimental data.

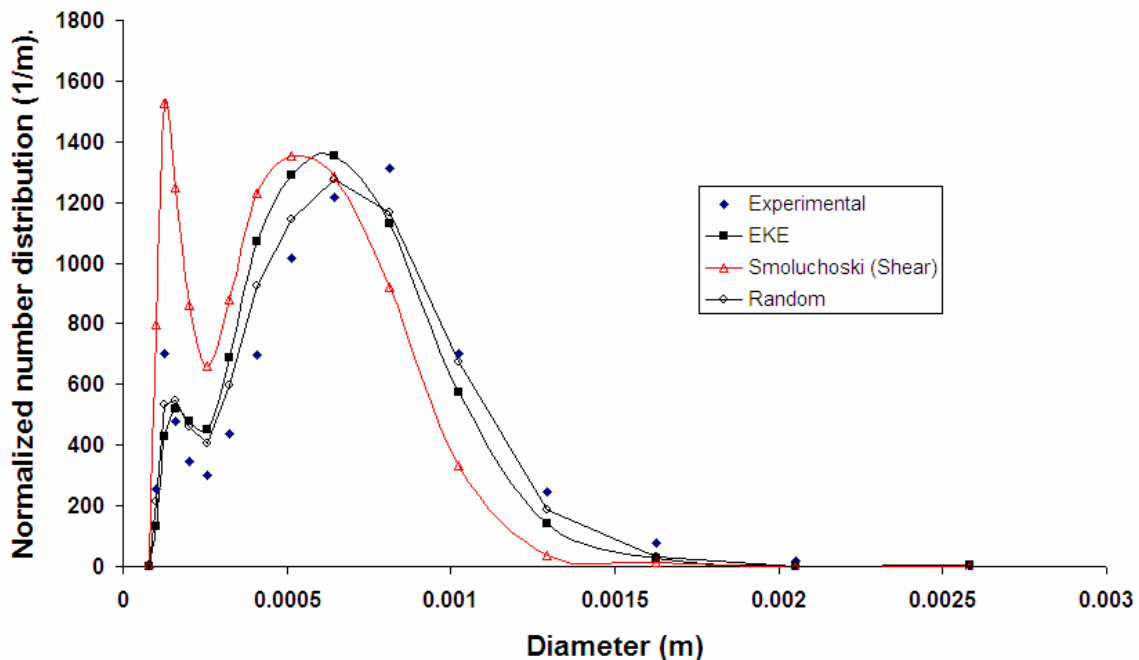


Figure 4.3 Fitting the coalescence kernels to the experimental data of wet granulation of medium size powders (PSD3) at 13.6 %v/w of binder with 1 cp viscosity. Simulated (line) and experimental (rhombus). The end of experiment (12 minutes).

Table 4.3 Fitting the coalescence kernels to the experimental data

<i>Kernel structure</i>	<i>fundamental</i>	<i>Residual: Bimodal PSD</i>
$\beta_0(t)(l + \varepsilon)^3$	Shear flow	4.0120×10^{-1}
$\beta_0(t)(l + \varepsilon)^2 \times \sqrt{\left(\frac{1}{l^3} + \frac{1}{\varepsilon^3}\right)}$	Equipartition of kinetic energy.	1.7822×10^{-1}
$\frac{C}{\mu} \frac{(l + \varepsilon)^2}{(l \times \varepsilon)}$	Diffusion theory	1.2482×10^{-1}

Next, the parameter value was used to predict the experiment replicate carried out at the same conditions. The simulation results describe the PSD experimental during the wet granulation with good agreement as demonstrated in Figure 4.4. The PSD experimental data match the simulation during the first 8 minutes, but tend to diverge towards the end of the experiment. This is due to the decrease in the number of small particles and the increase in the particle size, which does not favor the assumptions of collision between small and large particles, and random motion of minute particles immersed in a fluid, respectively. The same parameter value was also used to predict the growth kinetics of wet granulation of medium size powders (PSD2) at 13.6 %v/w of binder and 1 cp, as shown in Figure 4.5. The initial PSD is a powder property and a process variable that affect the growth rate [14, 29]. This effect was incorporated into the PBE coalescence kernel by assuming preferential collision between small and large particles as explained in previous section. The simulation results describe the experimental data with good agreement.

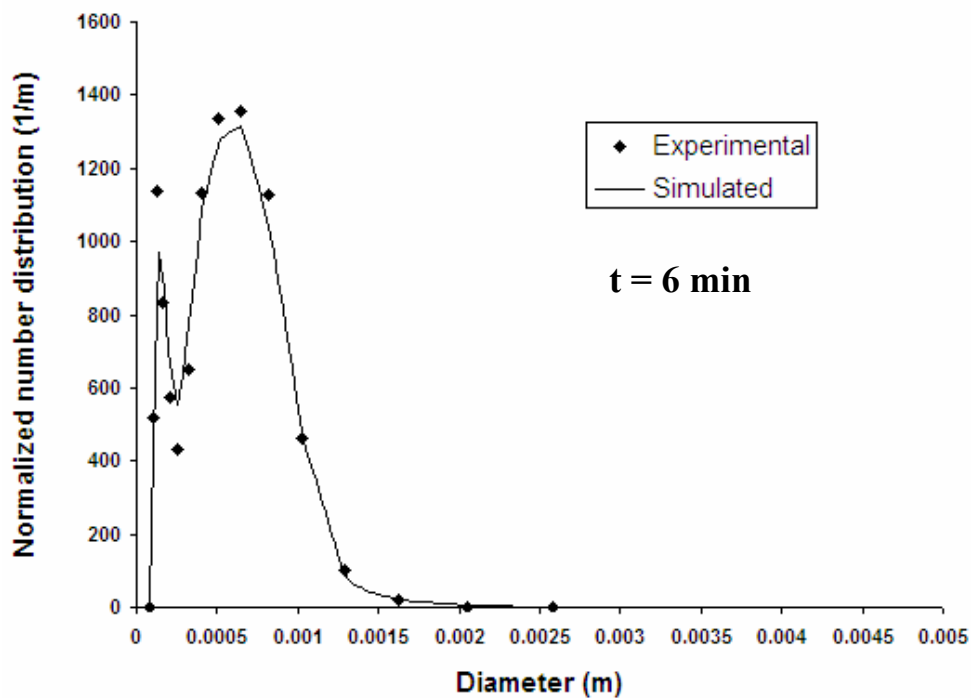
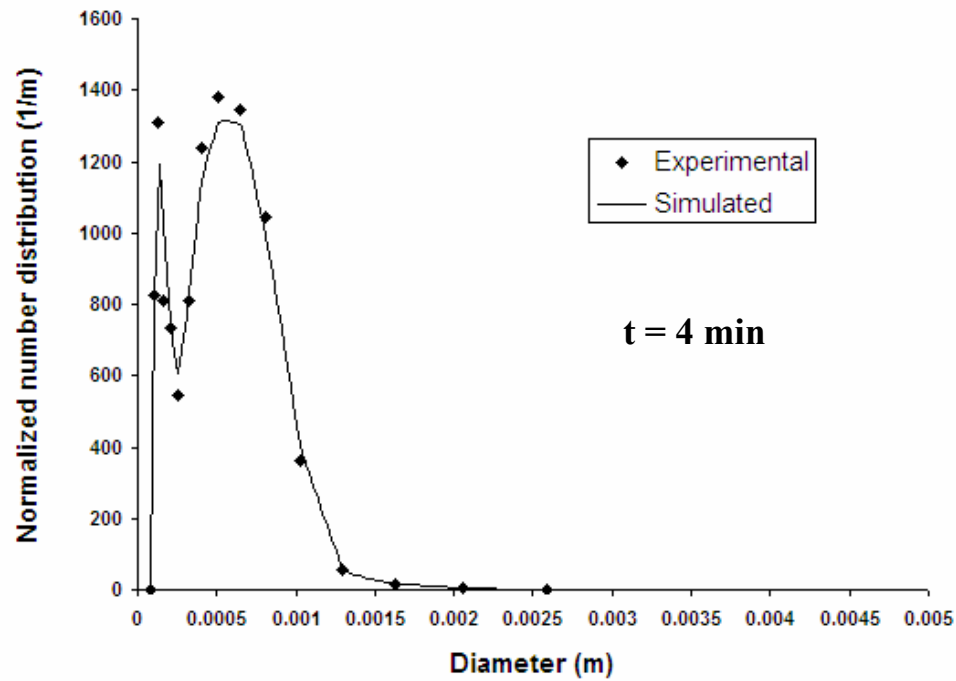


Figure 4.4 Prediction of the growth kinetics of wet granulation of coarse size powders (PSD3) at 13.6 %v/w of binder with 1 cp viscosity. Simulated (line) and experimental (rhombus).

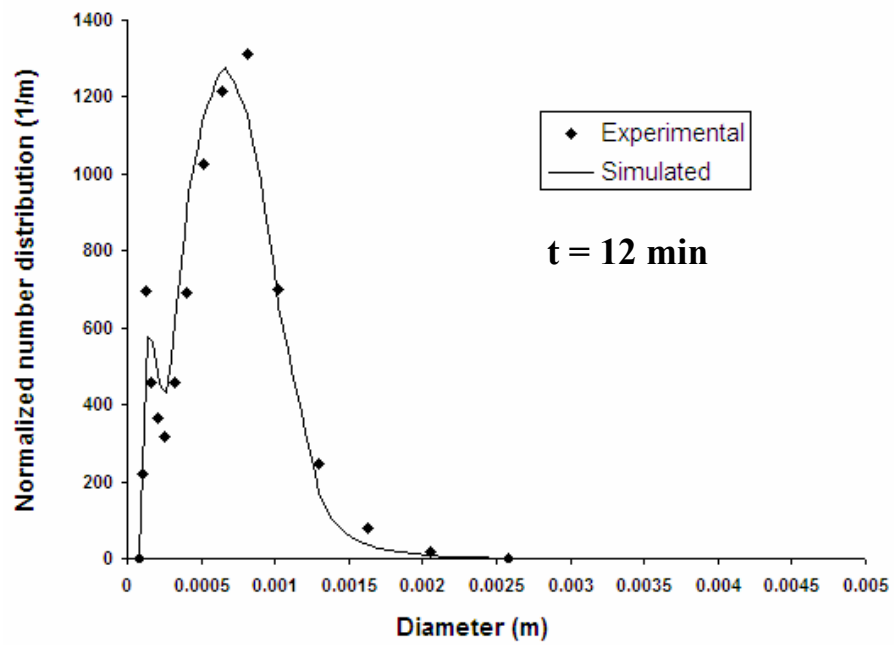
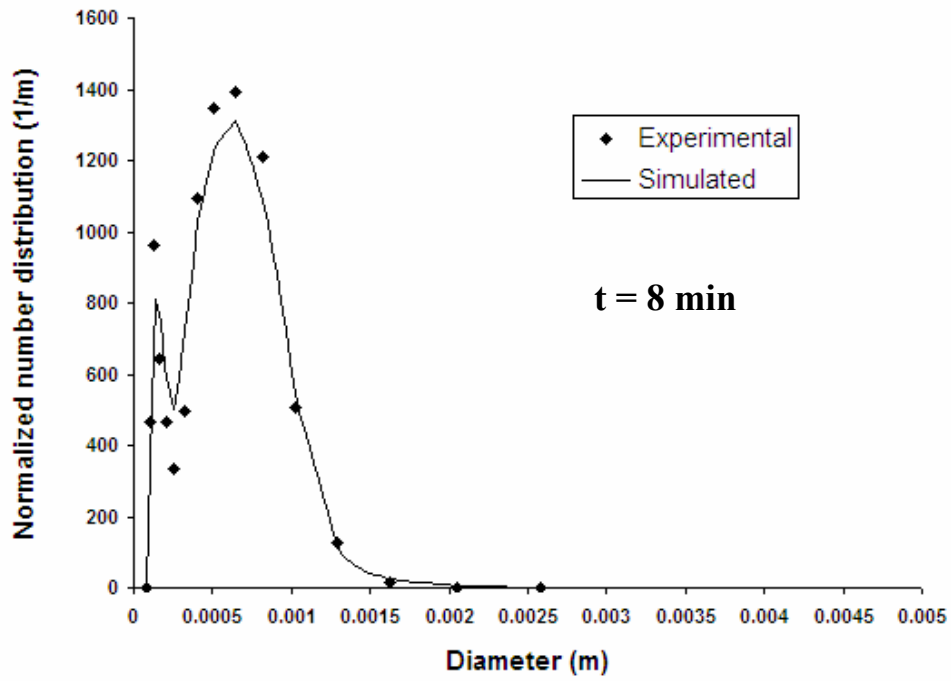


Figure 4.4 (Continued)

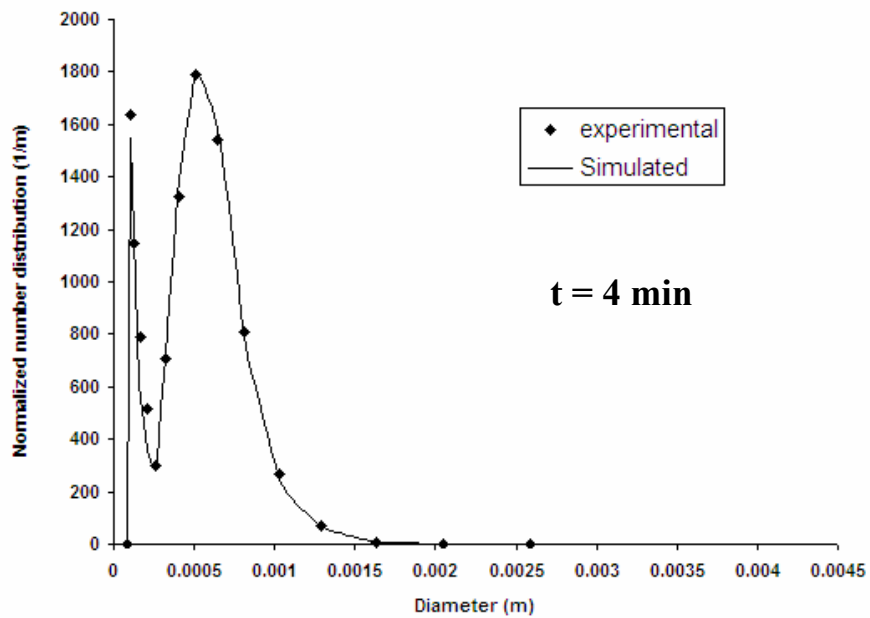
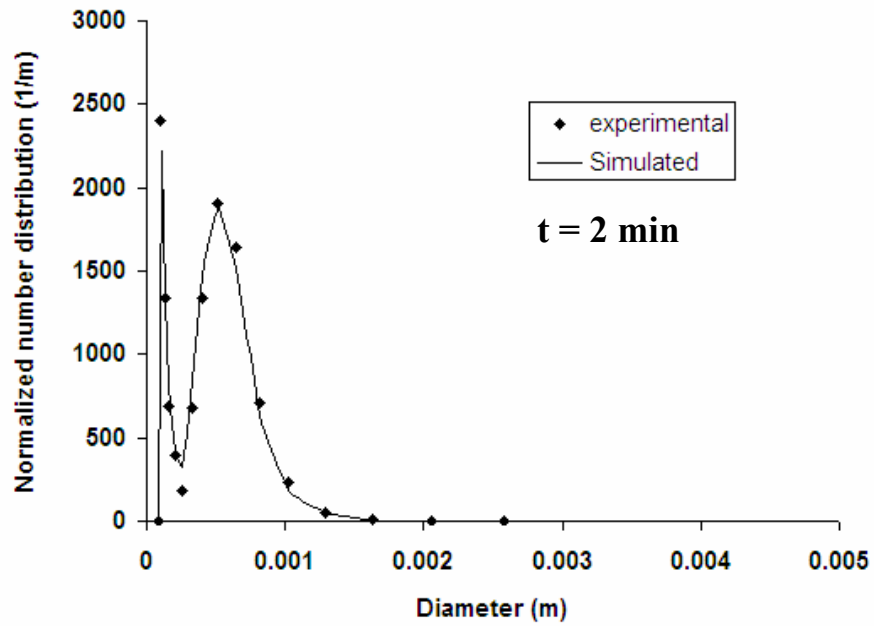


Figure 4.5 Prediction of the growth kinetics of wet granulation of medium size powders (PSD2) at 13.6 %v/w of binder with 1 cp viscosity. Simulated (line) and experimental (rhombus)

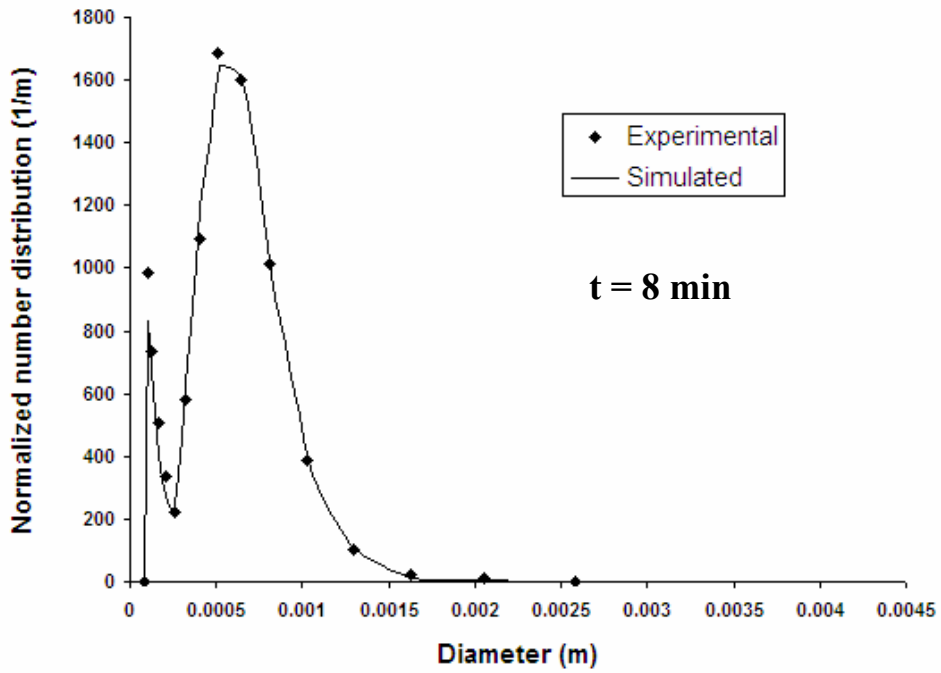
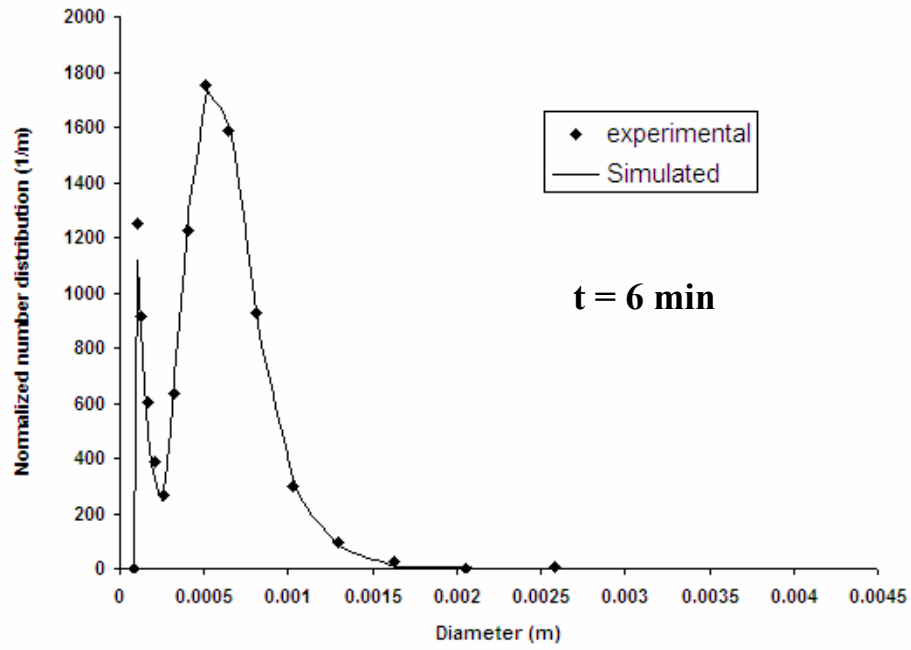


Figure 4.5 (Continued)

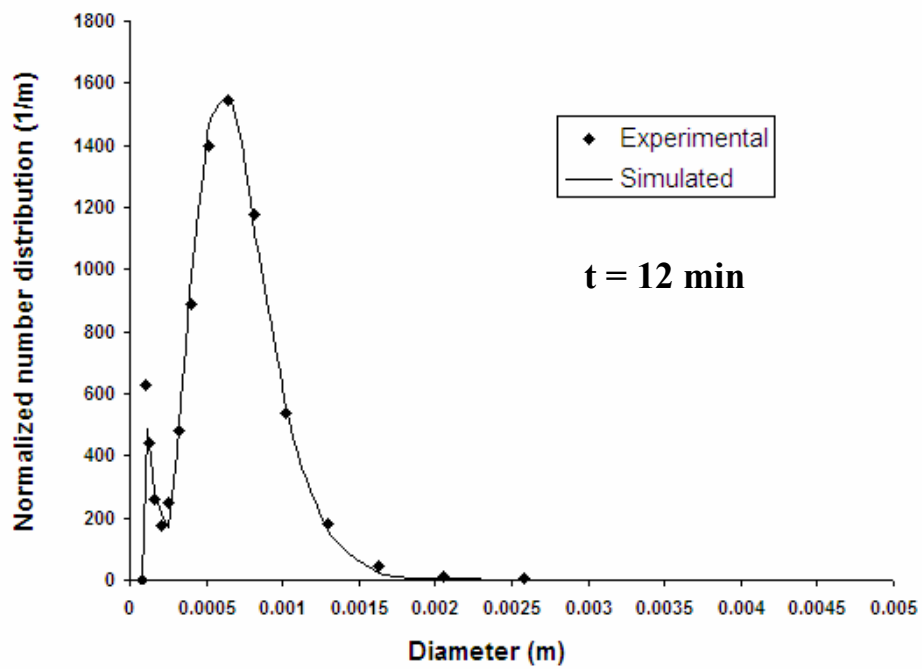
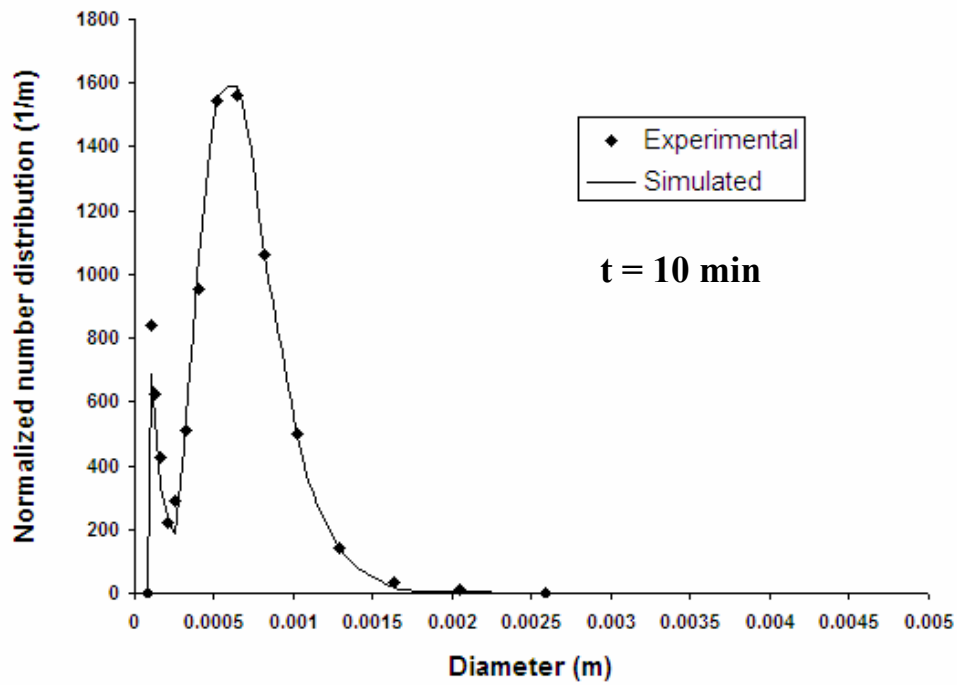


Figure 4.5 (Continued)

4.5 Conclusions

A sequential mechanism consisting of two stages (fast and low) has been observed during the wet granulation of powders with bimodal PSD, which presents a volume ratio of about 150 between small and large particles. Thus, agglomeration between small and large particles was considered based on diffusion of small particle to a large one through the binder layer on the particle's surface. Furthermore, coalescence kernels with physical interpretation have been developed for each stage to predict the growth kinetics of wet granulation, from initial properties of powder and binder such as particle size and binder viscosity. The kernel simulation for first stage predicts the trend of fast growth but it is necessary additional inline measurements to reduce perturbations in the wet granulation process during the first minute and so as to analyze this complex mechanism. The simulation results describe the PSD experimental during second stage of wet granulation with good agreement by assuming preferential agglomeration between small and large particles.

REFERENCES

- [1] B. Ennis, Unto Dust Shalt Thou Return. 1997. *Powder & Grains*, Behringer and Jenkins, eds., Balkema, Rotterdam **97**, pp. 13-23.
- [2] L. Aboud and S. Henry. September 12, 2003. New prescription for drug makers: Update the plants. *Wall Street Journal*.
- [3] J. Carroll January 2, 2005. Stand PAT. Available from www.spectroscopyonline.com
- [4] D. Randolph and M. Larson. 1971. *Theory of Particulate Processes*. Academic Press. New York, United States.
- [5] M. Taylor. 2002. Quantitative measures for shape and size of particles. *Powder Technology*, 124, pp. 94-100.
- [6] V. Mikli, H. Kaerd, P. Kulu, M. Besterici. 2001. Characterization of powder particle morphology. *Proceeding of Estonian Acad. Sci. Eng.*, **7(1)**, pp. 22-34.
- [7] K. Belaroui, M. Pons, H. Vivier. 2002. Morphological characterisation of gibbsite and alumina. *Powder Technology*, 127, pp. 246-256.
- [8] M. Pons, H. Vivier, V. Delcour, J. Authelin, L. Pailleres-Hubert. 2002. Morphological analysis of pharmaceutical powders. *Powder Technology*, **128**, pp. 276-286.
- [9] General Test <776>, "Optical Microscopy," *USP 24* (The United States Pharmacopoeias Convention, Rockville, MD, 2000), pp. 1965–1967.
- [10] R. Gonzalez, R. Woods. 1993. *Digital Image Processing*. Addison-Wesley. New York, United States.
- [11] Y. Anzai. 1992. *Pattern Recognition and Machine Learning*. Academia Press, INC. Yokohama, Japan, pp. 123-175.
- [12] M. Hu. 1961. Pattern recognition by moment invariant. *Proceeding of Institute of Radio Engineers (IRE)*, **49**, p. 1428.
- [13] M. Hu. 1962. Visual Pattern recognition by moment invariant. *IRE Transactions on Information Theory*, **IT-8**, pp. 179-187.

- [14] M. Mackaplow, L. A. Rosen, and J. N. Michaels. 2000. Effect of primary particle size on granule growth and endpoint determination in high-shear wet granulation. *Powder Technology*, **108**, pp. 32-45.
- [15] C. Cai, and D. Radspinner. A novel approach to determining particle size distributions of pharmaceutical powders by near infrared spectroscopy. *American Pharmaceutical Review*, **8(6)**, pp. 51-56.
- [16] S. Watano, K. Miyanami. 1995. Image processing for on-line monitoring of granule size distribution and shape in fluidized bed granulation. *Powder Technology*, **83**, pp. 55-60.
- [17] D. Montgomery. 2001. *Design and Analysis of Experiments*. John Wiley 7 Sons, Inc. New York, United States, pp. 519-548.
- [18] K. Castleman. 1979. *Digital image processing*. Prentice-Hall, Inc., Englewood Cliffs, N. J., United States, pp. 150-156.
- [19] M. Teague. 1979. Image analysis via the general theory of moments. *Journal of the Optical Society of America*, **70(8)**, pp. 920-930.
- [20] C. Teh, R. Chin. 1988. On image analysis by the method of moments. *IEEE Transactions on Pattern Analysis and Machine Intelligent*. **10(4)**, pp. 496-513.
- [21] D. Zhang, G. Lu. 2002. A Comparative Study of Three Region Shape Descriptors. *Digital Image Computing Techniques and Applications*, **21-22**, pp. 1-6.
- [22] Guideline for Industry, Test on Validation of Analytical Procedures. 1995. Available from <http://www.fda.gov/cder/guidance/ichq2a.pdf>, ICH-Q2A.
- [23] M. Parker, R. Rowe. 1991. Source variation in the wet massing (granulation) of some microcrystalline celluloses. *Powder Technology*, **65**, pp. 273-281.
- [24] C. Cape. 1980. Particle size enlargement. *Handbook of Powder Technology*, **1**, Elsevier, Amsterdam.
- [25] B. Ennis, G. Tardos, and R. Pfeffer. 1991. A microlevel-based characterization of granulation phenomena. *Powder Technology*, **65**, pp. 257-272.
- [26] B. Ennis, G. Tardos, and R. Pfeffer. 1990. The influence of viscosity on the strength of an axially strained pendular liquid bridge. *Chemical Engineering Science*, **45**, pp. 3071-3088.

- [27] P. Mill, J. Seville, P. Knight and M. Adams. 2000. The effect of binder viscosity on particle agglomeration in a low shear mixer/agglomerator. *Powder Technology*, **113**, pp. 140-147.
- [28] A. Adetayo, J. Litster, S. Pratsinis, and B. Ennis. 1995. Population balance modelling of drum granulation of materials with wide size distribution. *Powder Technology*, **82**, pp. 37-49.
- [29] S. Badawy and M. Hussain. 2004. Effect of starting particle size on its agglomeration behavior in high shear wet granulation. *AAPS PharmSciTech*, **5** (3) Article 38.
- [30] G. Tardo, M. I. Khan, and P. R. Mort. 1997. Critical parameters and limiting conditions in binder granulation of fine powders. *Powder Technology*, **94**, pp. 245-258.
- [31] M. Hounslow, J. M. K. Pearson and T. Instone. 2001. Tracer studies of high-shear granulation: II. Population balance modeling. *AIChE Journal*, **47** (9), pp. 1984-1998.
- [32] R. Boerefijn and M. Hounslow 2005. Studies of fluid bed granulation in an industrial R&D context. *Chemical Engineering Science*, **60**, pp. 3879-3890.
- [33] A. Realpe, and C. Velázquez. 2006. Pattern recognition for characterization of pharmaceutical powders. *Powder Technology*, 169, Issue 2, 108-113.
- [34] J. Duckworth. 1998. *Spectroscopic quantitative analysis*. In: Workman J, Springsteen A, eds. *Applied Spectroscopy: A Compact Reference for Practitioners*. San Diego, CA: Academic Press, pp. 93-163.
- [35] I. Jolliffe. 1986. *Principal component analysis*. Springer-Verlag, INC. New York, United States
- [36] J. Workman, P. Mobley, B. Kowalski and R. Bro. 1996. Review of chemometrics applied to spectroscopy: 1985-95, part I. *Applied Spectroscopy Review*, **31**(1&2), pp. 73-124.
- [37] A. Jægerskou, P. Holm, T Schaefer and H. Kristensen. 1984. Granulation in high speed mixers. Part 3: Effects of process variables on the intragranular porosity. *Pharm. Ind.*, **46**(3): p. 310-314
- [38] P. Holm, O. Jungersen, T. Schaefer and H. Kristensen. 1984. Granulation in high speed mixers: Part 1. Effects of process variables during kneading. *Pharm. Ind.*, **46**, pp. 97-101.

- [39] N. Lindberg. 1984. Granulation of lactose in a domestic type mixer. *Drug dev. Ind. Pharm*, **10**, pp. 45-56.
- [40] T. Schæfer, Holm, P., Kristensen, H.G., 1990a. Wet granulation in a laboratory scale high shear mixer. *Pharm. Ind.* **52**, 1147-1153.
- [41] F. Hoornaert, P. A. Wauters, G. M. Meesters, S. E. Pratsinis, and B. Scarlett. 1998. Agglomeration Behaviour of Powder in a Lodige Mixer Granulator. *Powder Technology*. **96**, pp. 116-128.
- [42] S. Schaafsma, P. Vonk, P. Segers, N. Kossen. 1998. Description of agglomerate growth. *Powder Technology*, **97**, pp. 183-190.
- [43] P. Holm, O. Jungersen, T. Schaefer and H. Kristensen. 1983. Granulation in high speed mixers: Part 1. Effects of process variables during kneading. *Pharm. Ind.*, **45**, pp. 806-811.
- [44] M. Smoluchowski. 1917. Mathematical theory of the kinetics of the coagulation of colloidal solutions, ' Z. *Phys. Chem.*, **92**, pp. 129-168.
- [45] M. Wulkow, A. Gerstlauer, U. Nieken. 2001. Modeling and simulation of crystallization processes using Parsival. *Chemical Engineering Science*, **56**, pp. 2575–2588.
- [46] H. Hulburt and S. Katz. 1964. Some problem in particle technology. A statistical mechanical formulation. *Chemical Engineering Science*, **19**, pp. 555-574.
- [47] K. Satry, and D. Fuerstenau. 1973. Mechanisms of agglomerate growth in pelletization. *Powder Technology*, **7**, pp. 97-111.
- [48] M. Cliff. 1990a. Granulation End Point and Automated Process Control of Mixer-Granulators: Part I. *Pharmaceutical Technology*, **14** (4), pp. 112-129.
- [49] M. Cliff. 1990b. Granulation End Point and Automated Process Control of Mixer-Granulators: Part II. *Pharmaceutical Technology*, **14** (5), pp. 38-44.
- [50] M. Golovin. 1963. The solution of the coagulation equation for raindrops, taking condensation into account. *Soviet. Physics. Dokl.*, **8(2)**, pp. 191-193
- [51] P. Kapur. 1972. Kinetics of Granulation by Nonrandom Coalescence Mechanism. *Chemical Engineering Science*, **27**, pp. 1863-1869.

- [52] A. Einstein. 1905. On the movement of small particles suspended in stationary liquids. *Ann. Physik.*, **17**, pp. 549-560.
- [53] A. Einstein. 1956. *Investigations on the theory of the Brownian movement*. Edited by R. Fürth, translated by A. Cowper. Dover Publications, Inc. New York, United States.
- [54] G. Uhlenbeck. and L. Ornstein. 1930. On the theory of the Brownian motion. *Physical Review*, **36**, pp.823-841.
- [55] P. Kapur and D. Fuerstenau. 1969. A coalescence model for granulation. *I&EC Process design and Development*, **8(1)**, pp. 56-62.
- [56] P. Langevin. 1908. *On the theory of Brownian motion*. C. R. Acad. Sci. (Paris), **146**, pp. 530-533.
- [57] N. Wax. 1954. *Selected paper on noise and stochastic processes*. Dover Publications, Inc. New York, United States.

5 RECOMMENDATIONS AND FUTURE WORK

5.1 Recommendations

It is suggested to put a small blade in top of mixer to reduce stagnant zone in the granulator, when granulation experiments are carried out at 12 %v/w of binder content with 2.45 cp viscosity or higher, as indicated in Figure 5.1.

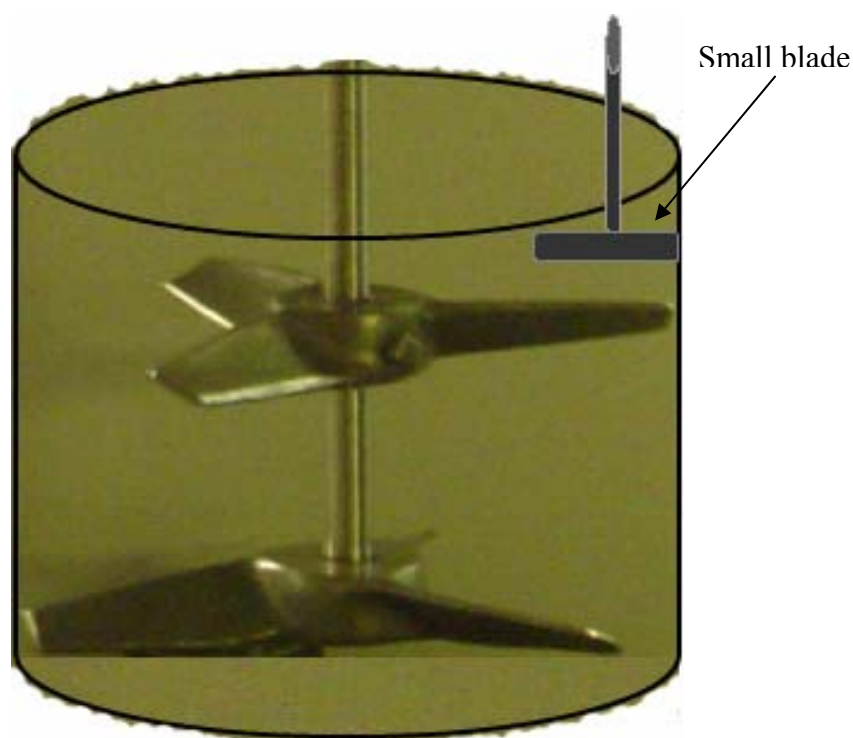


Figure 5.1 Granulator schematic

The granulator blades must only promote the collision between particles, not cut particles, neither to press the granules against vessel wall.

Scale-up is recommended if an acceptable mixing quality is obtained inside granulator to reduce spatial variation in PSD. Although, several small granulators of high shear could be

considered to obtain reliable results, because this process is relatively fast. Thus, increase the manufacturing efficient with the goal of ensuring final product quality.

5.2 Future Work

Wet granulation in a high shear mixer is a complex process, in which several mechanisms, breakage and agglomeration, could occur of separated, simultaneous or sequential way, depending upon the variation of one or more factors such as initial particle size, initial PSD shape (unimodal versus bimodal), and viscosity and the amount of binder. It shows why the wet granulation process after many years of research is still not completely understood. In this thesis a fundamental understanding of the effect of initial PSD shape (unimodal or bimodal) on agglomeration mechanism in wet granulation was carried out. However, it is recommended to understand the breakage mechanism, to obtain a suitable breakage kernel for the PBE.

The first stage of wet granulation is fast and short. It would be necessary to obtain more samples during the first two minutes of wet granulation to calculate more accurate parameters by fitting the experimental data. The non-invasive inline measurements of PSD or to take samples automatically without stopping the granulator are recommended to reduce perturbations in the granulation process. Although, the setup of inline method to create a non-invasive process interface is in itself a science, where different aspects, such as overlapping of particles, movement of the material, placement of the interface and dirtying of lens during the granulation process, have to be considered.

APPENDIX A. Calibration Model for Moisture Content Determination

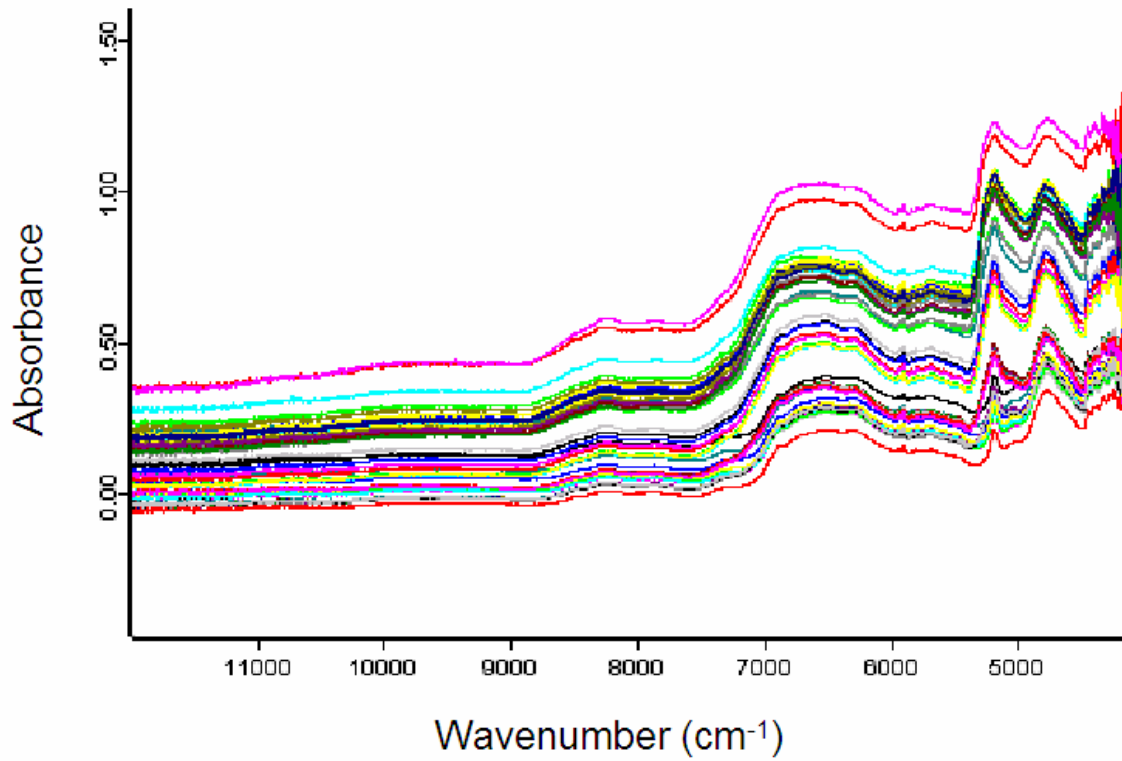


Figure A.0.1 Absorbance spectra for moisture calibration model of lactose-water mixture

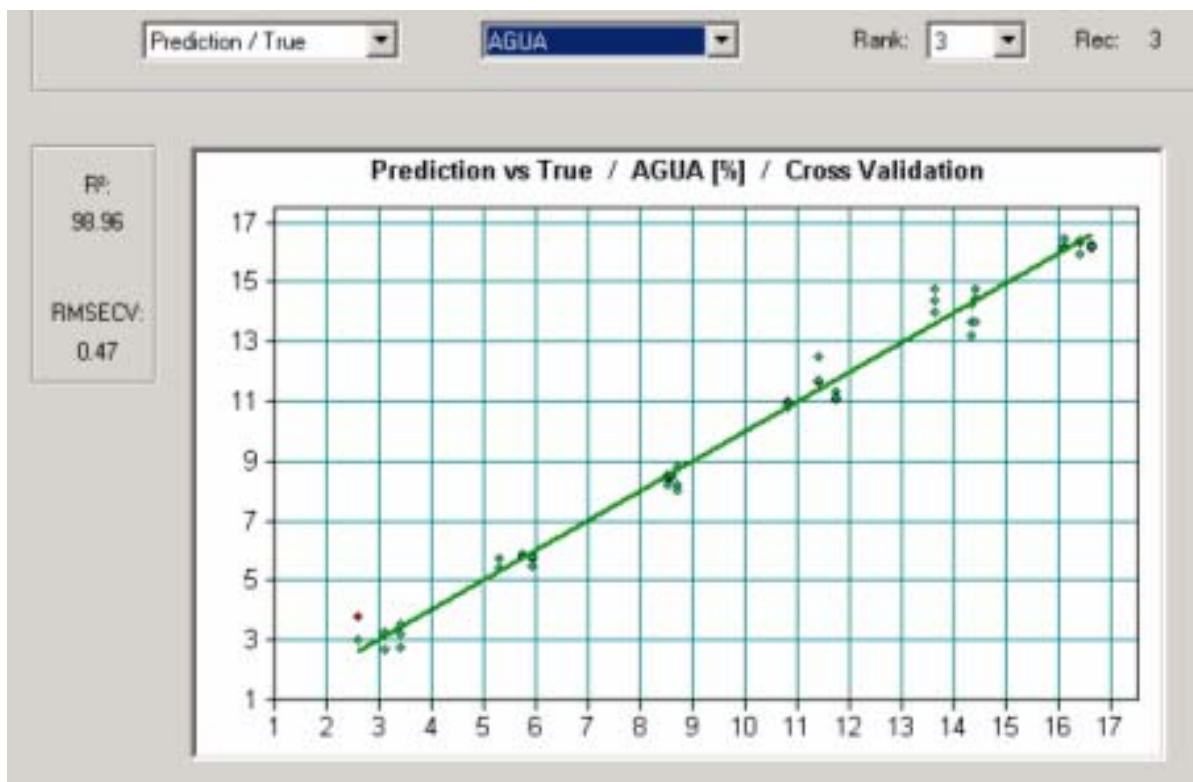


Figure A.0.2 Calibration model for lactose-water mixture

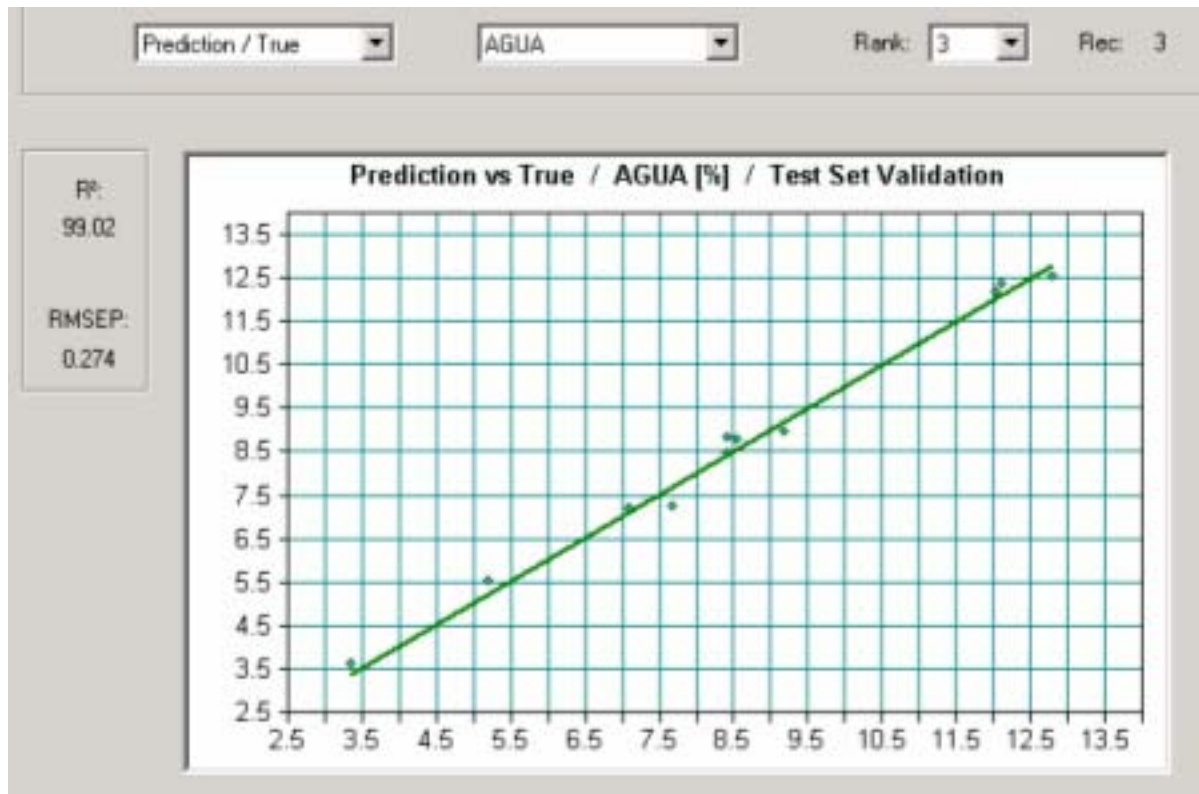


Figure A.0.3 Validation model for lactose-water mixture

APPENDIX B. Mass Median Diameter (MMD)

Table B.0.1 Mass median diameter for each combination of factors and levels

Sample conditions	Sample MMD (mm)	Replicate MMD (mm)
PSD3-9.9-1	0.4496	0.4524
PSD3-9.9-2.49	0.4484	0.4463
PSD3-9.9-4.85	0.4478	0.4395
PSD3-11.7-1	0.4619	0.4592
PSD3-11.7-2.49	0.4518	0.4627
PSD3-11.7-4.85	0.4740	0.4692
PSD3-13.6-1	0.8081	0.7979
PSD3-13.6-2.49	0.9421	0.8973
PSD3-13.6-4.85	0.8518	0.9253
PSD2-9.9-1	0.3471	0.3498
PSD2-9.9-2.49	0.3410	0.3432
PSD2-9.9-4.85	0.3421	0.3396
PSD2-11.7-1	0.3691	0.3743
PSD2-11.7-2.49	0.4383	0.4392
PSD2-11.7-4.85	0.4549	0.4482
PSD2-13.6-1	0.7598	0.7569
PSD2-13.6-2.49	0.8590	0.8142
PSD2-13.6-4.85	0.7566	0.7938
PSD1-9.9-1	0.1573	0.1642
PSD1-9.9-2.49	0.1556	0.1547
PSD1-9.9-4.85	0.1543	0.1553
PSD1-11.7-1	0.1624	0.1629
PSD1-11.7-2.49	0.1621	0.1634
PSD1-11.7-4.85	0.1643	0.1714
PSD1-13.6-1	0.2673	0.2589
PSD1-13.6-2.49	0.2125	0.2754
PSD1-13.6-4.85	0.2502	0.2248

Sample condition meaning (PSD1-13.6-2.49): The first term indicates the particle size distribution as shown in Figure 3.2, the second term indicate the binder content (% v/w), and the third term indicates the binder viscosity (cp).

Table B.0.2 Analysis of variance (ANOVA) for mass median diameter measurements

Analysis of Variance (ANOVA) for MMD

Source	DF	Seq SS	Adj SS	Adj MS	F	P
Binder Viscosity	2	0.00581	0.00581	0.00291	9.810	0.001
Binder Content	2	1.11544	1.11544	0.55772	1881.380	0.000
Particle Size	2	1.65930	1.65930	0.82965	2798.680	0.000
Binder Viscosity*Binder Content	4	0.00789	0.00789	0.00197	6.650	0.001
Binder Viscosity*Particle Size	4	0.00562	0.00562	0.00141	4.740	0.005
Binder Content*Particle Size	4	0.28861	0.28861	0.07215	243.390	0.000
Binder Viscosity*Binder Content* Particle Size	8	0.01056	0.01056	0.00132	4.450	0.002
Error	27	0.00800	0.00800	0.00030		
Total	53	3.10124				

SD = 0.0172175 (mm)

R-Sq = 99.74%

R-Sq(adj) = 99.49%